mouse displayed a distinct response profile compared with control animals harboring either the C57BL/6 *Ahr* allele ($Ahr^{b\text{-}1}$) (TCDD-sensitive C57BL/6J AHR) or the DBA/2 *Ahr* allele (Ahr^{d}) (TCDD-resistant DBA/2 AHR) in the same C57BL/6J genetic background. Although gene expression responses mediated by hAHR from 3-MC were comparable to that by DBA/2 AHR, the homozygous human AHR knock-in allele (h*AHR*) mouse was the weakest responder to TCDD among the three strains examined. These results suggest that hAHR molecules expressed in mice retain a functional human specificity that can be distinguished from the murine AHR and provide important insights into the toxicological susceptibility of humans to AHR ligands released into the environment.

Materials and Methods

Construction of the hAHR Knock-in Vector. The hAHR knock-in vector was constructed by using 129SV/J mouse *Ahr* genomic clones and hAHR cDNA as described (22). A 2-kb *Bam*HI/*Hph*I fragment containing the 129SV/J *Ahr* promoter was ligated to the hAHR cDNA (9, 22). The *neo* gene cassette was fused to the 3′ end of the hAHR cDNA in a reverse orientation, followed by a 6.5-kb *Hind*III/*Eco*RI fragment of the 129SV/J *Ahr* gene. This construct was ligated to the thymidine kinase cassette on the 5′ end.

Generation of hAHR Knock-in Mice. The knock-in vector was electroporated into E14 embryonic stem (ES) cells (23). A pair of primers (sense, GTATGCATTACCATGCTCCCATTCTGCTGG; antisense, ACATCTTGTGGGAAAGGCAGCAGGCTAGCC) was used for PCR screening. After confirmation by Southern blot analysis, positive clones were injected into blastocysts. Heterozygous hAHR knock-in mice were backcrossed into a C57BL/6J background up to the seventh generation and interbred to yield heterozygous and homozygous h*AHR* and wild-type $Ahr^{b\text{-}1/b\text{-}1}$ mice. The genotype of each pup was determined by PCR, with a common sense primer; 5′-ATGAGCAGCGGCGCCAACAT-3′, an antisense primer for endogenous *Ahr* allele; 5′-GCTAGACGGCACTAGGTAGG-3′, and an antisense primer for targeted allele; 5′-CAGGTAACTGACGCTGAGCC-3′. PCR amplification was carried out for 30 cycles under the following conditions; 94°C for 30 sec, 62°C for 30 sec, and 72°C for 30 sec.

Chemicals and Animals. TCDD (99.5% pure) and 3-MC were purchased from Cambridge Isotope Laboratories (Andover, MA) and Wako Pure Chemical (Osaka), respectively. D2N-*Ahrd* mice and inbred C57BL6/J mice were procured from The Jackson Laboratory. *Ahr*-null mutant mice used in this study were generated by Y.F.-K (22).

RNA Blotting Analyses. We isolated total RNA by using ISOGEN (Nippon Gene, Tokyo) and purified polyA RNA by using an Oligotex-MAG mRNA purification kit (Takara Biotechnology, Tokyo). For detection of Ahr mRNA, 5 μg of polyA RNA per lane was applied, and a portion of mouse $Ahr^{b\text{-}1}$ cDNA (*Bpu*1102I-*Kpn*I; 734-bp) encoding the PAS domain was used for a probe. This nucleotide sequence is conserved with 83% homology to the corresponding hAHR cDNA (12, 24). To examine the inducibility of *CYP1A1* and *CYP1A2*, 6-week-old littermates ($Ahr^{b\text{-}1/b\text{-}1}$ and homozygous h*AHR*) and D2N-*Ahrd* ($Ahr^{d/d}$) mice were given a single i.p. injection of 80 mg/kg 3-MC or 100 μg/kg TCDD. Mice were killed by cervical dislocation 24 h after injection. Ten micrograms of total RNA per lane was hybridized with the appropriate mouse cDNA probes (25).

RT-PCR Analyses of hAHR and Murine Ahr mRNA Expression in Embryos. Total RNA was isolated from palate and kidney of gestation day (GD)18.5 fetus by using ISOGEN. One microgram of the total RNA was reverse-transcribed into cDNA with Superscript-II reverse transcriptase (Life Technologies, Gaithersburg, MD) and random hexamers at 42°C for 50 min. The resulting cDNAs were subjected to 30 cycles of PCR by using the specific primers for the gene for the h*AHR* (5′ primer, 5′-GTAAGTCTCCCTTCATACC-3′; 3′ primer, 5′-AGGCACGAATTGGTTAGAG-3′), mouse *Ahr* (5′ primer, 5′-CTTTGCTGAACTCGGCTTGC-3′; 3′ primer, 5′-TTGCTGGGGGCACACCATCT-3′) and GAPDH (5′ primer, 5′-CCCCTTCATTGACCTCAACTACATGG-3′; 3′ primer, 5′-GCCTGCTTCACCACCTTCTTGATGTC-3′). The reaction was performed under the following conditions: 94°C for 30 sec, 60°C for 30 sec, and 72°C for 30 sec.

Immunohistochemical Analysis of hAHR Expression. Immunohistochemical analysis was performed as described (26). Lungs were fixed in 0.1 M phosphate buffer containing 4% paraformaldehyde for 24 h and embedded in paraffin. Sections were incubated with anti-AHR antibody in 1:200 dilution, which reacts with both human and mouse AHR (N-19; Santa Cruz Biotechnology). AHR immunoreactivity was visualized with the avidin-biotin-peroxidase system (Vector Laboratories).

TCDD Treatment and Evaluation of Teratogenesis. TCDD treatment was performed as described (22). On GD12.5, pregnant mice were given TCDD by i.p. administration at a dose of 40 μg/kg body weight (27). On GD18.5, the fetuses were taken out and fixed in 4% paraformaldehyde. The palatal structure was examined by cutting between the upper and lower jaws. The kidneys were sliced longitudinally and stained with hematoxylin/eosin. The presence and severity of hydronephrosis in each kidney was examined under a microscope as previously described (28) by using severity scores ranging from 0 to 3+ (0, normal kidney; 1+, slight decrease in length of papilla; 2+, marked decrease in length of papilla with some loss of renal parenchyma; 3+, complete absence of papilla, shell of kidney remaining with only a small amount of renal parenchyma). For statistical analysis, pairwise comparisons were made by Mann–Whitney *U* test, by using StatView for Macintosh version 5.0 (SAS Institute, Cary, NC).

Results

Replacement of the Mouse *Ahr* Gene with hAHR cDNA. We hypothesize that the specific functional characteristics of the hAHR molecule form the principal basis for the pattern of human responses to xenobiotics that interact with the AHR. To characterize responses mediated by hAHR, we generated a mouse possessing hAHR instead of murine AHR. hAHR cDNA was introduced into the mouse *Ahr* locus by homologous recombination, thereby disrupting the mouse *Ahr* gene (Fig. 1*A*). The cDNA was recombined so that hAHR is expressed under the control of the endogenous mouse *Ahr* promoter. Sixteen independent G418-resistant ES clones were obtained of 240 by PCR screening, and seven clones were further confirmed as correctly targeted ES cells by genomic DNA blot analysis. *Eco*RI-digested genomic DNA from the three representative positive clones (nos. 14, 25, and 58) revealed 11.0- and 6.2-kb fragments derived from the intact and targeted alleles, respectively, when hybridized with the 5′-external probe (Fig. 1*B*).

These three clones harboring h*AHR* were used for the generation of chimeric offspring. The male chimeras were mated with C57BL/6J females to obtain heterozygotes of the h*AHR* allele. They were subsequently bred into a C57BL/6J genetic background through the seventh generation, and the backcrossed heterozygous animals were interbred to yield hAHR homozygous mutant mice. The transmission of the targeted allele to the offspring was confirmed by genomic DNA blot analysis, and the genotype was determined by PCR by using tail DNA as a template (Fig. 1 *C* and *D*). Of 124 offspring obtained

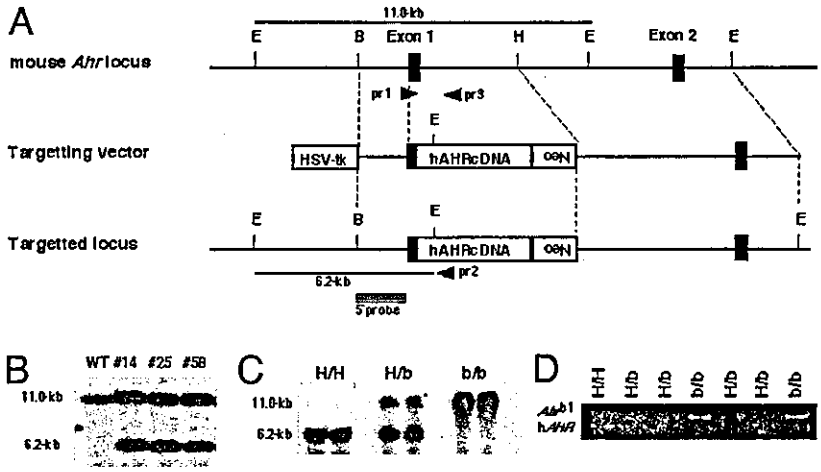

Fig. 1. Generation of the hAHR knock-in mouse. (*A*) Strategy for hAHR cDNA knock-in by homologous recombination. E, H, and B are restriction sites for *Eco*RI, *Hind*III, and *Bam*HI, respectively. Neo indicates the neomycin-resistance gene, and HSV-tk is the thymidine kinase gene under control of the herpes simplex virus promoter. The 5′-genomic probe used for DNA blot analysis is indicated by the hatched box. The positions of wild-type (pr 3) and mutant allele-specific (pr 2) primers and the common primer (pr 1) used in the genotyping PCR are indicated by arrowheads. The *Eco*RI restriction fragments detected with the 5′-genomic probe in the wild-type and targeted allele are denoted by horizontal bars. (*B*) DNA blot analyses of three recombinant ES clones. Genomic DNA was prepared from the ES clones (nos. 14, 25, and 58), and aliquots (10 μg) were digested by *Eco*RI. *Eco*RI digestion generated 11.0- and 6.2-kb bands for the wild-type and targeted alleles, respectively, by using the 5′-genomic probe. (*C*) Genotyping of the *Ahr* gene by DNA blot analysis. Genomic DNA was extracted from the tails of heterozygous and homozygous h*AHR* mice and wild-type $Ahr^{b\text{-}1/b\text{-}1}$ mice and digested by *Eco*RI for DNA blot analysis. (*D*) Genotyping of littermates from the intercrosses of heterozygotes. PCR fragments of wild-type amplified with pr1 and pr3 ($Ahr^{b\text{-}1}$; 280 bp) and mutant allele with pr1 and pr2 (h*AHR*; 240 bp) as depicted in *A*. H/H, H/b, and b/b indicate homozygous and heterozygous h*AHR* mice and wild type ($Ahr^{b\text{-}1/b\text{-}1}$), respectively.

from heterozygous matings, wild-type ($Ahr^{b\text{-}1/b\text{-}1}$), heterozygous, and homozygous h*AHR* mutant mice numbered 29, 71, and 24, respectively, conforming to the expected Mendelian inheritance ratio. Homozygous h*AHR* mice were viable, and no abnormalities were observed.

Expression of hAHR in hAHR Knock-in Mice. The expression of hAHR and mouse Ahr mRNAs was examined by RNA blot analysis by using polyA RNAs isolated from major AHR-expressing organs including liver, lung, kidney, intestine, and thymus (Fig. 2*A*). A cDNA fragment encoding the PAS domain of C57BL/6 AHR, which shows 83% homology with the corresponding human molecule, was used as a common probe for detecting both mouse Ahr and hAHR mRNAs. The larger band detected in heterozygous h*AHR* mice and wild-type $Ahr^{b\text{-}1/b\text{-}1}$ mice corresponds to the 5.4-kb transcript derived from the endogenous $Ahr^{b\text{-}1}$ gene, and the shorter 5.0-kb transcript observed in heterozygous and homozygous h*AHR* is derived from the hAHR knock-in allele. This result establishes that, whereas the homozygous h*AHR* mouse lacks mRNA for murine *Ahr*, it expresses mRNA for h*AHR*. Further, the level of expression of hAHR mRNA is comparable to that of endogenous murine Ahr mRNA in the other strains.

The embryonic expressions of mouse Ahr and hAHR mRNAs were examined by RT-PCR at the stage of GD18.5. As observed in the RNA blot analysis of adult tissues, the hAHR mRNA was expressed in the embryonic palate and kidney of homozygous and heterozygous h*AHR* mice. The abundance was comparable with that of the mouse Ahr mRNA expressed in $Ahr^{b\text{-}1/b\text{-}1}$ and heterozygous h*AHR* mice (Fig. 2*B*). These results demonstrate that hAHR mRNA is transcribed under the control of the mouse *Ahr* promoter in both adult and embryonic hAHR knock-in mice.

To ascertain that hAHR protein is expressed from the knock-in allele, immunohistochemical analysis was performed on lung sections obtained from hAHR knock-in homozygous mouse and the *Ahr*-null mutant (22). Intense signals were detected in the alveolar epithelial cells of hAHR knock-in animals (Fig. 2*C*). The signal intensity of *Ahr*-null mutant lung (Fig. 2*D*) was as faint as the hAHR knock-in lung without the antibody (data not shown). Thus, hAHR protein is expressed from the knock-in allele.

The hAHR Knock-in Mouse Displays a Distinct Induction Profile of AHR Target Genes to Different AHR Ligands. The response of the hAHR knock-in mouse to two prototypical AHR ligands, 3-MC and TCDD, was examined. To characterize the distinct properties, if any, of the hAHR, two strains of control mice were used for the analysis. One strain is a wild-type mouse in the C57BL/6J genetic background, which possesses AHR with high affinity for TCDD. The other strain is a congenic mouse, D2N-*Ahrd*, possessing AHR with low affinity (from DBA/2 mouse) in the C57BL6J genetic background. Because the hAHR knock-in mouse was backcrossed into C57BL/6J, these two strains of mouse enabled us to compare the characteristics of hAHR to those of C57BL/6J and DBA/2 AHR in the same genetic background.

Robust expression of the *CYP1A1* and *CYP1A2* genes was observed in the liver of $Ahr^{b\text{-}1/b\text{-}1}$ mice after administration of 3-MC, whereas the magnitudes of induction in homozygous h*AHR* and $Ahr^{d/d}$ mice were much weaker and comparable to each other (Fig. 3*A*). The relative mean band intensities for *CYP1A1* were 1.0 and 0.9 and were 1.0 and 1.1 for *CYP1A2* in homozygous h*AHR* and $Ahr^{d/d}$ mice, respectively. After treatment with TCDD, the induction of the two genes was strongest in $Ahr^{b\text{-}1/b\text{-}1}$ mice, intermediate in $Ahr^{d/d}$ mice, and weakest in homozygous h*AHR* mice (Fig. 3*B*). The fold inductions in homozygous h*AHR*, $Ahr^{d/d}$, and $Ahr^{b\text{-}1/b\text{-}1}$ mice were 1.0, 4.9, and 14.6 for *CYP1A1*, and 1.0, 5.7, and 8.4 for *CYP1A2*, respectively.

When the responses of $Ahr^{b\text{-}1/b\text{-}1}$ and $Ahr^{d/d}$ mice were compared, the *CYP1A1* expression levels were higher in $Ahr^{b\text{-}1/b\text{-}1}$ than in $Ahr^{d/d}$ mice, which is consistent with previous reports (9, 12, 13). It is noteworthy that the responsiveness of homozygous h*AHR* mice to 3-MC was almost comparable to that of $Ahr^{d/d}$ mice, whereas the responsiveness to TCDD was much weaker. The differential response between $Ahr^{d/d}$ and homozygous h*AHR* mice was unexpected, because a previous study indicated

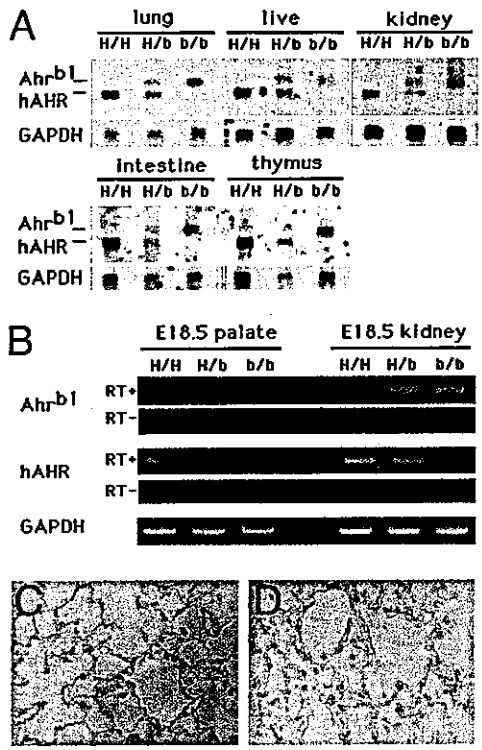

Fig. 2. Expression of hAHR in multiple tissues of the hAHR knock-in mouse. (*A*) RNA blot analysis of polyA RNA (5 μg/lane) extracted from five representative organs of homozygous and heterozygous h*AHR* mice and $Ahr^{b\text{-}1/b\text{-}1}$ mice. Human and mouse *Ahr* transcripts (hAHR and $Ahr^{b\text{-}1}$, respectively) are indicated (*Left*). The same membrane was rehybridized with ^{32}P-labeled cDNA of mouse *GAPDH*. H/H, H/b, and b/b are described in the Fig. 1 legend. (*B*) RT-PCR analyses of hAHR and murine Ahr mRNA expression in kidney and palate of GD18.5 fetuses. The reverse transcription was conducted either in the presence (+) or absence (−) of reverse transcriptase. PCR products representing the transcripts derived either from h*AHR* or $Ahr^{b\text{-}1}$ are indicated on the left. (*C* and *D*) Immunohistochemical analysis of hAHR protein in the lung of a homozygous h*AHR* mouse. Immunoreactivity of AHR protein was observed in the alveolar epithelial cells of homozygous h*AHR* lung (*C*), whereas no immunoreactivity was observed in the lung of $Ahr^{-/-}$ mouse (*D*). Original magnifications, ×400 (*C* and *D*).

that hAHR and DBA/2 AHR exhibit similar dissociation constants for TCDD binding as measured *in vitro* (9, 19). This result suggests that ligand binding does not fully define the integrated function of hAHR.

hAHR Knock-in Mouse Is Relatively Resistant to TCDD-Induced Teratogenicity. The responses to TCDD mediated by hAHR are weaker than that by DBA/2 and C57BL/6 AHR when measured

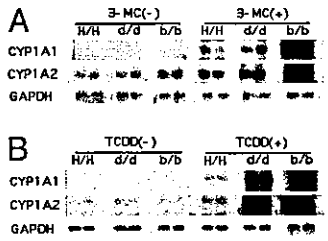

Fig. 3. Inducible expression of AHR target genes. Northern blot analysis of AHR-regulated *CYP1A1* and *CYP1A2* was performed. Six-week-old homozygous h*AHR*, $Ahr^{d/d}$, and $Ahr^{b\text{-}1/b\text{-}1}$ mice were treated with 80 mg/kg 3-MC (*A*) or 100 μg/kg TCDD (*B*). Total hepatic RNA was isolated 24 h after treatment and subjected to Northern analysis (10 μg/lane). Equal loading was confirmed by the abundance of *GAPDH* transcripts.

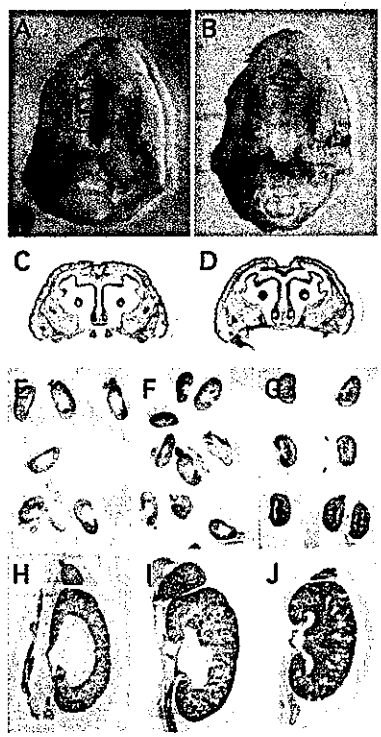

Fig. 4. Fetal teratogenesis after maternal administration of TCDD. (*A* and *C*) Cleft palate in an $Ahr^{b\text{-}1/b\text{-}1}$ fetus is shown. Filled arrowheads in *A* and open arrowheads in *C* indicate the failure of palatine shelves to fuse. Note that homozygous h*AHR* fetuses showed no cleft palates after TCDD treatment (*B* and *D*). (*E*, *F*, *H*, and *I*) Fetal hydronephrosis induced by TCDD. $Ahr^{b\text{-}1/b\text{-}1}$ (*E* and *H*) and homozygous h*AHR* (*F* and *I*) fetuses are shown. (*G* and *J*) Unaffected kidneys from untreated $Ahr^{b\text{-}1/b\text{-}1}$ fetuses are shown.

as inducibility of *CYP1A* family genes. Teratogenicity is a more integrated and complex toxicological manifestation of TCDD action. The most prominent teratogenic effects of TCDD on mouse fetus are cleft palate and hydronephrosis, both of which depend completely on AHR expression (29). The frequency and severity of these teratogenic effects of TCDD were examined in hAHR knock-in fetuses. Homozygous hAHR knock-in females were mated with males of the same genotype and given a single i.p. dose of 40 μg of TCDD per kg of body weight at GD12.5. $Ahr^{b\text{-}1/b\text{-}1}$ and $Ahr^{d/d}$ females were treated in the same way as controls. All dams were weighed to monitor the normal continuation of the pregnancy and killed at GD18.5 to remove fetuses for examination of cleft palate and hydronephrosis.

As reported previously, cleft palate was observed in 100% of the wild-type $Ahr^{b\text{-}1/b\text{-}1}$ fetuses exposed to TCDD (Fig. 4 *A* and *C* and Table 1) (22). By contrast, none of the treated homozygous h*AHR* fetuses showed abnormal palatogenesis (Fig. 4 *B* and *D* and Table 1). An intermediate frequency (30%) of cleft palate was observed in the $Ahr^{d/d}$ fetuses. Differences in the severity of cleft palate were not apparent in any of the symptomatic fetuses of any genotype. This anomaly was most frequent in $Ahr^{b\text{-}1/b\text{-}1}$, intermediate in $Ahr^{d/d}$, and least frequent in homozygous h*AHR* mice, in accordance with the transcriptional inducibility of AHR target genes, which was strongest in $Ahr^{b\text{-}1/b\text{-}1}$, intermediate in $Ahr^{d/d}$, and weakest in homozygous h*AHR* mice. Thus, a strong correlation between the incidence of cleft palate in each strain and the intrinsic transcriptional activity of their respective AHR molecules was observed.

Hydronephrosis, another teratogenic effect of TCDD, is characterized by a dilated renal pelvis. The severity of this anomaly in the fetal kidney was scored from 0 (normal) to 3 (severest)

Table 1. Incidence of anomalies caused by TCDD in homozygous h*AHR*, $Ahr^{b\text{-}1/b\text{-}1}$, and $Ahr^{d/d}$ fetuses

Genotype of fetuses	TCDD dose, μg/kg	Dams examined, *n*	Fetuses examined, *n*	Fetuses with: Cleft palate *n*	Cleft palate %*	Hydronephrosis *n*	Hydronephrosis %*	Hydronephrosis Severity: 0–3.0†
$Ahr^{b\text{-}1/b\text{-}1}$	0	2	13	0	0	2	12.5	0.19 ± 0.10‡
$Ahr^{b\text{-}1/b\text{-}1}$	40	5	29	29	100	26	89.7	2.54 ± 0.14§
$Ahr^{d/d}$	0	2	15	0	0	2	13.3	0.20 ± 0.10‡
$Ahr^{d/d}$	40	5	30	9	30	25	81.7	1.98 ± 0.14§
Homo-h*AHR*	0	2	16	0	0	1	6.3	0.03 ± 0.03‡
Homo-h*AHR*	40	5	37	0	0	30	81.1	1.19 ± 0.01§

*Percentage of fetuses with each anomaly of all fetuses examined.
†The criteria for severity scores are described in *Materials and Methods*. Data are expressed as mean ± SE.
‡Significant difference between TCDD-treated and -untreated fetuses of each genotype ($P < 0.0001$).
§Significant difference between TCDD-treated homozygous h*AHR* fetuses and $Ahr^{b\text{-}1/b\text{-}1}$ or $Ahr^{d/d}$ fetuses ($P < 0.0001$).

according to criteria described previously (28). When kidneys scored at 1, 2, or 3 were counted as hydronephrotic, 89.7% of the $Ahr^{b\text{-}1/b\text{-}1}$ offspring suffered from this teratogenic outcome after TCDD treatment (Fig. 4 *E* and *H*, and Table 1 for TCDD-treated animals; Fig. 4 *G* and *J*, and Table 1 for untreated animals). A similar incidence was observed in a previous study (22). $Ahr^{d/d}$ and homozygous h*AHR* fetuses also displayed this teratogenic effect with incidences of 81.7% and 81.1%, respectively (Fig. 4 *F* and *I*, and Table 1). Thus, there is no substantial difference in the incidence of hydronephrosis among the mice expressing the three distinct *Ahr* (h*AHR*) genes. When severity score values were compared among the TCDD-treated fetuses, they averaged 2.54, 1.98, and 1.19 for the $Ahr^{b\text{-}1/b\text{-}1}$, $Ahr^{d/d}$ and homozygous h*AHR* genotypes, respectively (Table 1). Therefore, hydronephrosis observed in the homozygous h*AHR* fetuses was significantly less severe compared with that in either $Ahr^{b\text{-}1/b\text{-}1}$ or $Ahr^{d/d}$ fetuses. Nonetheless, the average score of TCDD-treated homozygous h*AHR* fetuses (1.19) was still significantly higher than that of untreated homozygous h*AHR* fetuses (0.03), clearly demonstrating that the TCDD-activated hAHR mediates renal teratogenesis in mice. Although the magnitude of *CYP* gene induction is dramatically different depending on the *Ahr* genotype, the incidence of hydronephrosis is surprisingly comparable among the three strains. These results revealed that differences between human and murine AHR allowed for the emergence of discrete biological effects; e.g., hydronephrosis, but not cleft palate in homozygous h*AHR* mice.

To exclude the possibility that maternal factors affect the teratogenic manifestations on the fetuses, heterozygous h*AHR* parents were used to obtain homozygous h*AHR* and $Ahr^{b\text{-}1/b\text{-}1}$ fetuses. Heterozygous mothers were treated with TCDD as described above, and fetuses were examined for both cleft palate and hydronephrosis. As described in Table 2, the incidence of cleft palate was 100% and 0% in $Ahr^{b\text{-}1/b\text{-}1}$ and homozygous h*AHR* fetuses, respectively, which is identical to the results presented in Table 1. The incidence and severity (mean score) of hydronephrosis were 100% and 2.47 for $Ahr^{b\text{-}1/b\text{-}1}$ and 66.6% and 1.17 for homozygous h*AHR* fetuses, respectively. Again, a more moderate effect in the homozygous h*AHR* fetuses is suggested, the severity difference being statistically significant. Therefore, we conclude that the TCDD-induced teratogenic effects are independent of maternal genotypes, and that fetal AHR activity is critical for determining the outcomes.

Discussion

One of the central issues in the uncertainty surrounding risk assessments for TCDD and its structural analogs is whether humans are relatively sensitive or resistant to the toxicities of this class of compounds. Because the pleiotropic adverse effects induced by these toxins involve multiple processes, the human response is generated by the summation and integration of the properties inherent to the human components, including expression level, ligand-binding affinity, and transcriptional activity of the AHR, as well as the variety, function and activity of the AHR target genes. Through numerous preceding studies, the primary structure of the AHR protein has been regarded as one of the most critical factors determining the susceptibility and specificity of responses of animals to various PAH/HAHs including dioxin. On the basis of several observations *in vitro*, polymorphic variation in the *Ahr* gene is considered the primary basis for differences in sensitivity to TCDD among strains of mice (9–11). In this study, we attempted to establish an *in vivo* system to evaluate the specific function of the hAHR protein to better evaluate its role in determining possible patterns of human responses to PAH/HAHs.

For this purpose, we adopted a knock-in strategy to introduce hAHR cDNA into the mouse *Ahr* genomic locus by homologous recombination. This strategy offers an obvious advantage compared with a transgenic method, because the introduced sequence is transcribed under the same regulatory mechanisms of the replaced gene (30). As desired, expression levels of the h*AHR* transcript were almost the same with those of endogenous mouse

Table 2. Incidence of anomalies caused by TCDD in fetuses from heterozygous h*AHR* parents

Genotype of fetuses	TCDD dose, μg/kg	Dams examined, *n*	Fetuses examined, *n*	Fetuses with: Cleft palate *n*	Cleft palate %*	Hydronephrosis *n*	Hydronephrosis %*	Hydronephrosis Severity: 0–3.0
$Ahr^{b\text{-}1/b\text{-}1}$	40		9	9	100	9	100.0	2.47 ± 0.14†
Hetero-h*AHR*	40	7	25	12	48	22	88.0	2.46 ± 0.13
Homo-h*AHR*	40		12	0	0	8	66.6	1.17 ± 0.01†

*Percentage of fetuses with each anomaly out of all fetuses examined.
†Significant difference between homozygous h*AHR* and $Ahr^{b\text{-}1/b\text{-}1}$ fetuses ($P < 0.0001$).

Ahr mRNA in multiple AHR-expressing tissues of adult mice and GD18.5 embryos. The hAHR protein was detected by immunostaining in the lungs of homozygous h*AHR* mice.

A possible explanation of the relative resistance of the hAHR knock-in mouse to TCDD lies in the qualitative difference between the human and mouse AHR molecules. Assuming that the abundance of the hAHR protein is the same as that of the endogenous mouse AHR, our results imply that the hAHR-mediated response to TCDD *in vivo* is much lower than that of DBA/2 AHR, although previous reports showed that their affinities to TCDD, as measured *in vitro*, are almost the same (9, 19). Alignment of the primary amino acid sequences of the two molecules indicates the considerable divergence in the C-terminal regions (9) and the deletion analysis differently localized the transcriptional activity within the regions (31). Such structural diversity of the C-terminal region might lead to species-specific interaction behaviors with transcriptional cofactors. TCDD-activated hAHR may not recruit coactivators as efficiently as the DBA/2 counterpart. One possibility must be noted that the incompatibility between TCDD-activated hAHR and the mouse coactivators may cause the reduced response of hAHR knock-in mouse to TCDD.

hAHR was not detectable by immunoblot analysis with the current antiserum, and its abundance relative to the constitutive level of mouse AHR protein could not be determined. Considering this lack of quantitative information, limited protein accumulation might account for the attenuated responsiveness of hAHR knock-in mice to TCDD. hAHR may have an intrinsically shorter life than mouse AHR at physiological expression levels *in vivo*.

The susceptibility of embryonic kidneys of homozygous h*AHR* mice to the teratogenic effects of TCDD is noteworthy. The pathogenesis of this renal lesion induced by TCDD involves hyperplasia of the ureteric epithelium, resulting in an occlusion of the ureter and subsequent hydronephrosis (32). Adverse effects on the kidney and urinary tract have also been reported in humans exposed to TCDD (33). However, studies in Ben Tre Province in Vietnam, where defoliant containing dioxin was sprayed extensively, revealed little increase in the prevalence of cleft lip and/or palate compared with that observed in Japan (34), suggesting that hAHR is less potent to mediate the manifestation of cleft palate, and that a higher dose might be required for it. Consistent with these human reports, our analysis showed that hAHR, although expressed in mice, mediated the development of hydronephrosis induced by TCDD, but not cleft palate at our experimental dose. Thus, the knock-in animal seems to mimic some aspects of the human responses to PAH/HAHs.

An intriguing utilization of our knock-in mouse strategy would be as an *in vivo* system for the qualitative and quantitative assessment of possible human responses to various PAH/HAHs. In this study, D2N-*Ahrd* mice responded more strongly to TCDD than to 3-MC, whereas the hAHR knock-in mice responded almost equally to these two compounds. These results clearly show that the relative efficacy profiles, examined by TCDD and 3-MC, are different between D2N-*Ahrd* and our hAHR knock-in mouse. Therefore the efficacy profile specific to hAHR can be displayed by analyses of the responses of the hAHR knock-in mouse to an array of PAH/HAHs. Because environmentally relevant levels of exposure to dioxin and related compounds have garnered much concern in terms of their possible effects on reproductive, neurobehavioral, and immunological functions of humans, our hAHR knock-in mouse will serve as a humanized model mouse, exhibiting the human-specific responses to PAH/HAH congeners. This mouse should help define the range of biological and toxicological effects that could be expected to affect humans and thereby reduce some uncertainty in risk assessments of these persistent environmental contaminants.

We thank Drs. H. Ueda and S. Kimura at the Environmental Health Department of the Ministry of the Environment for valuable suggestions and support to initiate this project, and Dr. T. Kensler for the discussion and critical reading of the manuscript. We also thank Dr. N. Morito, Ms. N. Kaneko, and R. Kawai for help. This work was supported by grants from Exploratory Research for Advanced Technology Environmental Response Project (M.Y.), the Ministry of Education, Science, Sports and Culture (H.M. and M.Y.), the Ministry of Health, Labor, and Welfare (H.M., C.T., and M.Y.), Japan Society for the Promotion of Science–Research for the Future Program (M.Y.), Core Research for Evolutional Science and Technology (Y.F.-K., S.O., Y.A., C.T., and M.Y.), Program for Promotion Basic Research Activities for Innovative Biosciences (H.M. and S.T.), and Special Coordination Fund for Promoting Science and Technology (H.M.).

1. Poland, A. & Knutson, C. (1982) *Annu. Rev. Pharmacol. Toxicol.* **22**, 517–554.
2. Whitelock, J. P., Jr. (1990) *Annu. Rev. Pharmacol. Toxicol.* **30**, 251–277.
3. Landers, J. P. & Bunce, N. J. (1991) *Biochem. J.* **276**, 273–287.
4. Swanson, H. J. & Bradfield, C. A. (1993) *Pharmacogenetics* **3**, 213–230.
5. Hoffman, E. C., Reyes, H., Chu, F.-F., Sander, F., Conly, L. H., Brooks, B. A. & Hankinsin, O. (1991) *Science* **252**, 954–958.
6. Okey, A. B., Riddick, D. & Harper, P. A. (1994) *Toxicol. Lett.* **70**, 1–22.
7. Rowlands, J. & Gustafsson, J. A. (1997) *CRC Crit. Rev. Toxicol.* **27**, 109–134.
8. Poellinger, L. (2000) *Food Addit. Contam.* **17**, 261–266.
9. Ema, M., Ohe, N., Suzuki, M., Mimura, J., Sogawa, K., Ikawa, S. & Fujii-Kuriyama, Y. (1994) *J. Biol. Chem.* **269**, 27337–27343.
10. Poland, A. & Glover, E. (1990) *Mol. Pharmacol.* **38**, 306–312.
11. Poland, A., Palen, D. & Glover, E. (1994) *Mol. Pharmacol.* **46**, 915–921.
12. Ema, M., Matsushita, N., Sogawa, K., Ariyama, T., Inazawa, J., Nemoto, T., Ota, M., Oshimura, M. & Fujii-Kuriyama, Y. (1994) *J. Biochem.* **116**, 845–851.
13. Dolwick, K. M., Schmidt, J. V., Carver, L. A., Swanson, H. I. & Bradfield, C. A. (1993) *Mol. Pharmacol.* **44**, 911–917.
14. Okey, A. B., Vella, L. M. & Harper, P. A. (1989) *Mol. Pharmacol.* **35**, 823–830.
15. Pohjanvirta, R., Unkila, M. & Tuomisto, J. (1993) *Pharmacol. Toxicol.* **73**, 52–56.
16. Pohjanvirta, R., Wong, J. M. Y., Li, W., Harper, P. A., Tuomisto, J. & Okey, A. B. (1998) *Mol. Pharmacol.* **54**, 86–93.
17. Tuomisto, J. T., Viluksela, M., Pohjanvirta, R. & Tuomisto, J. (1999) *Toxicol. Appl. Pharmacol.* **155**, 71–81.
18. Mocarelli, P., Gerthoux, P. M., Ferrari, E., Patterson, D. G., Jr., Kieszak, S. M., Brambilla, P., Vincoli, N., Signorini, S., Tramacre, P., Carreri, V., *et al.* (2000) *Lancet* **355**, 1858–1863.
19. Micka, J., Milatovich, A., Menon, A., Grabowski, G. A., Puga, A. & Nebert, D. W. (1997) *Pharmacogenetics* **7**, 95–101.
20. Kohkalainen, M., Tuomisto, J. & Pohjanvirta, R. (2001) *Biochem. Biophys. Res. Commun.* **285**, 1121–1129.
21. Abnet, C. C., Tanguay, R. L., Heideman, W. & Peterson, R. E. (1999) *Toxicol. Appl. Pharmacol.* **159**, 41–51.
22. Mimura, J., Yamashita, K., Nakamura, K., Morita, M., Takagi, T. N., Nakao, K., Ema, M., Sogawa, K., Yasuda, M., Katsuki, M., *et al.* (1997) *Genes Cell.* **2**, 645–654.
23. Hooper, M., Hardy, K., Handyside, A., Hunter, S. & Monk, M. (1987) *Nature* **326**, 292–295.
24. Ema, M., Sogawa, K., Watanabe, N., Chujoh, Y., Matsushita, N., Gotoh, O., Funae, Y. & Fujii-Kuriyama, Y. (1992) *Biochem. Biophys. Res. Commun.* **184**, 246–253.
25. Fernandez-Salguero, P., Pineau, T., Hilbert, D. M., McPhail, T., Lee, S. S. T., Kimura, S., Nebert, D. W., Rudikoff, S., Ward, J. M. & Gonzalez, F. J. (1995) *Science* **268**, 722–726.
26. Moriguchi, T., Sakurai, T., Takahashi, S., Goto, K. & Yamamoto, M. (2002) *J. Biol. Chem.* **277**, 16985–16992.
27. Yasuda, M., Igarashi, E., Datu, A. R. & Igawa, H. (1986) *Teratology* 34, 454–455.
28. Birnbaum, L. S., Harris, M. W., Barnhart, E. R & Morrissey, R. E. (1987) *Toxicol. Appl. Pharmacol.* **90**, 206–216.
29. Birnbaum, L. S. & Abbott, B. (1997) in *Methods in Developmental Toxicology and Biology*, eds. Klug, S. & Thiel, R. (Blackwell Science, London), pp. 51–63.
30. Tsai, F. Y., Browne, C. P. B. & Orkin, S. H. (1998) *Dev. Biol.* **196**, 218–227.
31. Kumar, M. B., Ramadoss, P., Reen, R. K., Vanden Heuvel, J. P. & Perdew, G. H. (2001) *J. Biol. Chem.* **276**, 42302–42310.
32. Hoffman, R. E., Stehr-Green, P. A., Webb, K. B., Evans, R. G., Knutson, A. P., Schramm, W. F., Staak, J. L., Gibson, B. B. & Steinberg, K. K. (1986) *J. Am. Med. Assoc.* **255**, 2031–2038.
33. Abbott, B. D., Birnbaum, L. S. & Pratt, R. M. (1987) *Teratology* **35**, 329–334.
34. Natsume, N., Kawai, T. & Le, H. (1998) *Cleft Palate Craniofac. J.* **35**, 183–185.

THE JOURNAL OF BIOLOGICAL CHEMISTRY

Vol. 278, No. 24, Issue of June 13, pp. 21592–21600, 2003
Printed in U.S.A.

Keap1-dependent Proteasomal Degradation of Transcription Factor Nrf2 Contributes to the Negative Regulation of Antioxidant Response Element-driven Gene Expression*

Received for publication, January 28, 2003, and in revised form, March 29, 2003
Published, JBC Papers in Press, April 7, 2003, DOI 10.1074/jbc.M300931200

Michael McMahon‡, Ken Itoh§, Masayuki Yamamoto§, and John D. Hayes

From the Biomedical Research Centre, Ninewells Hospital and Medical School, University of Dundee, Dundee DD1 9SY, Scotland, United Kingdom and §Centre for Tsukuba Advanced Research Alliance and Institute of Basic Medical Sciences, University of Tsukuba, Tsukuba 305-8577, Japan

Keap1 is a negative regulator of Nrf2, a bZIP transcription factor that mediates adaptation to oxidative stress. Previous studies suggested this negative regulation is a consequence of Keap1 controlling the subcellular distribution of Nrf2. We now report that Keap1 also controls the total cellular level of Nrf2 protein. In the RL34 non-transformed rat liver cell line, Nrf2 was found to accumulate rapidly in response to oxidative stress caused by treatment with sulforaphane, and the accumulation resulted from inhibition of proteasomal-mediated degradation of the bZIP protein. By heterologously expressing in COS1 cells epitope-tagged Nrf2 and an $Nrf2^{\Delta ETGE}$ mutant lacking the Keap1-binding site, in both the presence and absence of Keap1 we demonstrate that Nrf2 is subject to ubiquitination and proteasomal degradation independently of both Keap1 and the redox environment of the cell. In oxidatively stressed cells, this is the sole mechanism responsible for Nrf2 degradation. However, under homeostatic conditions Nrf2 is subject to a substantially more rapid mode of proteasomal degradation than it is in oxidatively stressed cells, and this rapid turnover of Nrf2 requires it to interact with Keap1. Within Nrf2, the N-terminal Neh2 domain is identified as the redox-sensitive degron. These data suggest that Keap1 negatively regulates Nrf2 by both enhancing its rate of proteasomal degradation and altering its subcellular distribution.

Under homeostatic conditions, cells maintain their redox environment at a higher reducing potential than their surroundings (1). This is essential for correct biological function, and changes in the redox environment of the cell toward a more oxidized potential is referred to as oxidative stress. This can arise from exposure to pro-oxidant phytochemicals such as isothiocyanates, which react with GSH, and quinones, which can decouple mitochondrial electron transfer reactions, generating the superoxide anion (2, 3). Regardless of the source, oxidative stress, if prolonged, results in perturbation of cellular biochemistry and aberrant covalent modification of macromolecules, leading to tissue damage and DNA mutations.

Being disteleological, cells sense oxidative stress and respond by transcriptionally up-regulating numerous cytoprotective genes. These encode proteins with a variety of functions. For example, glutamate cysteine ligase catalytic and modifier subunits, glutathione reductase, malic enzyme 1, glucose-6-phosphate dehydrogenase, thioredoxin reductase, thioredoxin, peroxiredoxin MSP23, heme oxygenase 1, and the cystine/glutamate exchange transport system (4–9) act directly to replenish the cells major reductants. In addition, detoxication enzymes such as glutathione *S*-transferases, UDP-glucuronosyltransferases, aldo-keto reductases, and NAD(P)H:quinone oxidoreductase 1 (NQO1)[1] act indirectly by metabolizing and excreting the causative agents and byproducts of oxidative stress (10–12). Ferritin L chain (12) is induced and inhibits the ability of iron to catalyze the formation of reactive oxygen species. Genes encoding DNA damage repair enzymes might also be induced (8). Thus, in response to oxidants, the cell alters its biochemistry in many ways to reduce the potential for further oxidative stress, restore its redox balance, and repair damage accumulated during the stress. The antioxidant response element (ARE), a *cis*-acting element present in the promoters of many of the genes encoding the proteins listed above, provides a mechanism to explain their coordinated transcriptional regulation (for review, see Ref. 13).

Nrf2, a member of the "cnc" subfamily of bZIP transcription factors (for review, see Ref. 14), is an essential transactivator of genes containing an ARE, as evidenced by the marked impairment in the expression of genes encoding a number of detoxication enzymes and GSH biosynthetic enzymes in the liver and gastrointestinal tract of $nrf2^{-/-}$ mice (11, 15, 16). Nrf2 is highly conserved from mammalian species to chicken and Zebra fish, particularly within six regions designated the Neh1–6 (Nrf2-ECH homology) domains (17). The Neh1 domain contains the cnc-bZIP region, which dictates dimerization partners and confers DNA binding specificity. The Neh4 and Neh5 domains act cooperatively to bind the coactivator CREB-binding protein, thereby activating transcription (18). Of particular interest is the N-terminal region of ~100 amino acids, called the Neh2 domain, which negatively regulates Nrf2 function under homeostatic conditions (19) by mechanisms that are not fully understood.

* This work was funded by grants from the Association for International Cancer Research (99-041 and 02-049) (to M. Y. and J. D. H.). The TaqMan® analyses described herein were obtained with equipment provided by a Medical Research Council Cooperative Group Grant G0000281. The costs of publication of this article were defrayed in part by the payment of page charges. This article must therefore be hereby marked "*advertisement*" in accordance with 18 U.S.C. Section 1734 solely to indicate this fact.

‡ To whom correspondence should be addressed: Biomedical Research Centre, Ninewells Hospital and Medical School, Dundee DD1 9SY, Scotland, UK. Tel.: 44-1382-660111; Fax: 44-1382-669993; E-mail: m.j.m.mcmahon@dundee.ac.uk.

[1] The abbreviations used are: NQO1, NAD(P)H:quinone oxidoreductase 1; ARE, antioxidant response element; Neh, Nrf2-ECH homology; Keap1, Kelch-like ECH-associated protein 1; HA, hemagglutinin; Sul, sulforaphane; CAT, chloramphenicol acetyltransferase; CHX, cycloheximide; 2-ME, 2-mercaptoethanol; CREB, cAMP-response element-binding protein; CMV, cytomegalovirus.

The negative regulation of Nrf2 requires the interaction of the Neh2 domain with an actin-bound cytosolic protein, Keap1 (Kelch-like ECH-associated protein 1) (19). This appears to be a direct interaction as bacterially expressed and purified mKeap1 interacts *in vitro* with the Neh2 domain of mNrf2 (20). A tetrapeptide motif, ETGE, that resides close to the C-terminal boundary of Neh2 is critical for this phylogenetically conserved interaction (17). Itoh *et al.* (19) proposed that Keap1 negatively regulates Nrf2 function by controlling its subcellular localization. According to this model, Keap1 sequesters the bZIP protein in the cytoplasm under homeostatic conditions, leading to low expression of ARE-driven genes. During oxidative stress, a signal that involves phosphorylation and/or redox modification is transduced to the Keap1·Nrf2 complex (19–21), leading to its disruption and nuclear translocation of Nrf2. The increased level of nuclear Nrf2 results in enhanced occupancy of ARE enhancers by Nrf2/small Maf heterodimers, recruitment of CREB-binding protein, and transactivation of cytoprotective genes (18).

A drawback of this model is that it does not account for the apparent accumulation of total cellular Nrf2 in response to oxidative stress (22–25). Two research groups demonstrated that the accumulation of Nrf2 results from inhibition of its degradation by the 26 S proteasome (24, 25), a feature common to many transcription factors including p53, c-Myc, c-Jun, and β-catenin (26). In this study, we confirm that endogenous Nrf2 is subject to 26 S proteasome-dependent degradation and that its rate of degradation depends upon the redox environment of the cell. Importantly, we demonstrate that although Nrf2 is constitutively ubiquitinated and degraded by the proteasome, a direct interaction between the transcription factor and Keap1 confers redox sensitivity upon its half-life. Thus, under homeostatic conditions, Keap1 interacts with Nrf2 and increases its rate of proteasome-mediated degradation, leading to a reduction in the cellular levels of the bZIP protein. Oxidative stress, by antagonizing this interaction, stabilizes Nrf2, leading to its rapid accumulation within the cell. We identify the Neh2 domain of Nrf2 as the redox-sensitive degron.

EXPERIMENTAL PROCEDURES

Plasmids

Mouse Nrf2-expressing Plasmids—pcDNA3.1/V5HisBmNrf2 was generated by PCR amplification of the murine Nrf2 coding sequence and 50 nucleotides of 5′-untranslated region (27) using the primer pair 5′-CACAGCGTCCGCCCTCAGCATG-3′ and 5′-GTTTTTCTTTGTATCTGGCTTCTTGC-3′. The product was ligated into *Eco*RV-digested pcDNA3.1/V5HisB (Invitrogen), allowing expression of mNrf2-V5-his fusion protein from a CMV promoter. The pcDNA3.1/V5mNrf2, encoding mNrf2-V5, was generated from pcDNA3.1/V5HisBmNrf2 by site-directed mutagenesis using the primer 5′-GATTCTACGCGTACCGGTTAGCATCATCACCATCACCATTG-3′. Expression vectors pcDNA-3.1/V5HisBmNrf2$^{\Delta ETGE}$ and pcDNA3.1/V5mNrf2$^{\Delta ETGE}$ for mutant Nrf2, which lacks the ETGE tetrapeptide motif between residues 79 and 82 required for interaction with Keap1, were created by site-directed mutagenesis using the primer 5′-TTTTCGCTCAGTTTCAACTGGATGAATTCCTCCCAATTCAGCCGGCCC-3′. The pET15bmNrf2 plasmid encoding a hexahistidine-mNrf2 fusion protein was generated by PCR amplification of the mNrf2 coding sequence with the primer pair 5′-CCGCCCTCCATATGATGGACTTGGA-3′ and 5′-CTAAGAAATTAACTCGAGAGTTAAA-3′. The product was digested with *Nde*I and *Xho*I and ligated into *Nde*I/*Xho*I-digested pET15b (Novagen). The pCG-GAL(HA)mNeh2 plasmid, which expresses a hemagglutinin (HA)-tagged GAL4 DNA binding domain-mNeh2 fusion protein from a CMV promoter, was generated by PCR-amplification of the mNeh2 coding sequence (defined as the first 96 amino acids) using the primer pair 5′-CCTACCACAGCGTCCGCCTCTAGAATGATGGACTTGGAGTTGGC-3′ and 5′-CTGGGAGTAGCTGGCGGATCCTCAGGTGTCTGTCTGGATATGCTG-3′. The resulting product was digested with *Xba*I and *Bam*HI and ligated into similarly digested pCG-GAL(HA) (Ref. 28; kindly provided by Dr. William P. Tansey, Cold Spring Harbor Laboratory, NY). The pCG-GAL(HA)mNeh2$^{\Delta ETGE}$ vector was generated in an identical fashion, but a template expressing mNrf2$^{\Delta ETGE}$ was utilized for the PCR reaction.

Mouse Keap1-expressing Plasmids—A mKeap1 cDNA was generated by splice-overlap-extension of the PCR products amplified from two IMAGE consortium clones (315799, 5′-AGGCCCCTAACGGCTAGC-3′ and 5′-GCGTATAGCAGCCCACCC-3′; 988252, 5′-ACGCTGCACAAGCCCACG-3′ and 5′-CTGTTGTCAGTGCTCAGG-3′). The splice-overlap-extension product was cloned into pCRBlunt (Invitrogen) to generate pCRBluntmKeap1. The mKeap1 coding sequence was PCR-amplified from this template using two primers, 5′-TATGCAGCCCGAACCCAAGCTT-3′ and 5′-ATGCAGGTACAGTTTTGTTGATC-3′, and cloned into *Eco*RV-digested pcDNA3.1/V5HisC to generate pcDNA3.1/V5HisC-mKeap1, which expresses a mKeap1-V5-his fusion protein. The pcDNA-3.1/mKeap1 plasmid was generated from pcDNA3.1/V5HisCmKeap1 by site-directed mutagenesis using the primer 5′-CAAAACTGTACCTGCTGAATATCCAGCACAGTG-3′; this encodes mKeap1.

Miscellaneous—The p-164CAT and pARE-164CAT reporter constructs were gifts from Dr. Cecil B. Pickett (Schering Plough Research Institute, Kenilworth, NJ) and have been described previously (29). pCMVβ-gal (Clontech) expresses β-galactosidase under the control of a CMV promoter. pHisUb, which expresses hexahistidine-tagged octameric ubiquitin precursor protein from a CMV promoter (30), was provided by Prof. David P. Lane (University of Dundee). Site-directed mutagenesis was accomplished using the GeneEditor kit (Promega), according to the manufacturer's instructions. All constructs were sequence-verified.

Bacterial Expression and Purification of mNrf2

The pET15bmNrf2 plasmid was transformed into *Escherichia coli* BL21(DE3)RIL (Novagen) and selected on LB agar containing 100 μg/ml ampicillin and 34 μg/ml chloramphenicol. One colony was grown overnight at 37 °C in LB broth containing 200 μg/ml ampicillin and 34 μg/ml chloramphenicol. The next morning it was diluted 1:200 into 200 ml of LB broth containing 500 μg/ml ampicillin and 34 μg/ml chloramphenicol and grown at 37 °C to an $A_{600\ nm}$ of 0.4. Thereafter, the bacteria were harvested, and hexahistidine-mNrf2 was induced by resuspension in 200 ml of LB broth containing 500 μg/ml ampicillin, 34 μg/ml chloramphenicol, and 1 mM isopropyl-β-D-thiogalactopyranoside. The bacteria were incubated at 37 °C for 2 h, harvested, washed once with 50 mM Tris-Cl, pH 8.0, containing 2 mM EDTA, and resuspended in 5 ml of binding buffer (20 mM Tris-Cl, pH 7.9, 5 mM imidazole, 0.5 mM NaCl, and 0.01% (v/v) Nonidet P-40). Bacteria were lysed by the addition of 1 mg of lysozyme followed by incubation at 37 °C for 10 min. The lysate was flash-frozen, thawed by adding 20 ml of pre-warmed binding buffer, sonicated to reduce viscosity, and clarified by centrifugation (10,000 × *g*, 15 min, 4 °C). The resulting supernatant was sterile-filtered and applied to a 1-ml pre-charged Hi-Trap® Ni-chelate column (Amersham Biosciences). Hexahistidine-mNrf2 was eluted from the column in binding buffer supplemented with 250 mM imidazole, dialyzed against 50 mM Tris-Cl, pH 7.4, and flash-frozen and stored at −70 °C.

Cell Culture, Transfections, Chemical Challenge, and Reporter Assays

Both the RL34 non-transformed rat liver epithelial cell line (31) and COS1 cells were maintained in Dulbecco's modified Eagle's medium (Invitrogen) supplemented with 10% (v/v) heat-inactivated fetal calf serum (Invitrogen) and penicillin-streptomycin. Cells were seeded into either 6-well plates or 60-mm tissue culture dishes at least 18 h before transfection and were either 50% (RL34) or 90% (COS1) confluent at the time of transfection. Cells were transfected using Lipofectin (Invitrogen) according to the manufacturer's instructions. As an internal control, pCMVβ-gal was included in all transfections. Cells were chemically challenged not less than 40 h after plating. Sulforaphane (Sul) was obtained from LKT laboratories. Cycloheximide (CHX) was obtained from Sigma. Epoxomicin, *clasto*-lactacystin-β-lactone, and MG132 were obtained from Calbiochem. The β-galactosidase and chloramphenicol acetyl transferase (CAT) reporter assays were carried out as previously described (32).

Antibodies

During this study, a rabbit anti-mNrf2 antiserum was generated by immunization of a female New Zealand White rabbit with bacterially expressed hexahistidine-mNrf2 protein and was used at a dilution of 1:4000. Other antibodies were used at the following dilutions: rabbit anti-rNQO1, 1:3,000 (10); sheep anti-hUBF (upstream binding factor), 1:10,000 (Dr. Brian M. McStay, University of Dundee); rabbit anti-hMEK (mitogen-activated protein kinase-extracellular regulated ki-

nase), 1:1000 (Cell Signaling Technologies); sheep anti-hMnSOD (manganese superoxide dismutase), 1:1000 (Dr. Lesley I. McLellan, University of Dundee); rabbit anti-hCPR (cytochrome P450 reductase), 1:1000 (Dr. Mark J. I. Paine, University of Dundee); mouse anti-V5, 1:2000 (Invitrogen); mouse anti-HA, clone 12CA5, 0.4 μg/ml (Roche Applied Science).

Cell Extracts, Subcellular Fractionation, and Immunoblots

For immunoblots, whole-cell lysates were prepared by scraping cell monolayers into ice-cold radioimmune precipitation assay buffer (50 mM Tris-Cl, pH 7.4, 150 mM NaCl, 1% (v/v) Nonidet P-40, 0.5% (w/v) deoxycholic acid, 0.1% (w/v) SDS supplemented with Complete, EDTA-free protease inhibitor mixture (Roche Applied Science). Lysates were clarified by centrifugation (16,000 × *g*, 15 min, 4 °C).

Nuclear and 1000 × *g* supernatant fractions were prepared as follows. Monolayers in 60-mm dishes were trypsinized, and the cell suspension was washed with 3 volumes of ice-cold phosphate-buffered saline by repeated centrifugation (500 × *g*, 2 min, 4 °C.) The cell pellet was gently resuspended in 300 μl of STM-N buffer (250 mM sucrose, 50 mM Tris-Cl, pH 7.5, 5 mM $MgCl_2$, 10 mM iodoacetamide, 0.5% (v/v) Nonidet P-40 supplemented with Complete, EDTA-free protease inhibitor mixture). After 5 min on ice, the nuclei were pelleted (1000 × *g*, 5 min, 4 °C.) The resulting supernatant was harvested and is referred to as the 1000 × *g* supernatant. The nuclei were gently resuspended in 1 ml of STM buffer (STM-N, but lacking the Nonidet P-40) and layered onto 200 μl of a sucrose cushion (40% (w/v) sucrose, 10 mM HEPES, pH 7.5, 10 mM KCl, 1.5 mM $MgCl_2$, and 1 mM dithiothreitol) Nuclei were pelleted (1000 × *g*, 15 min, 4 °C) and lysed in 100 μl of ice-cold radioimmune precipitation assay buffer on ice for 15 min. The lysate was cleared by centrifugation (16,000 × *g*, 15 min, 4 °C), and the supernatant was harvested and is referred to as the nuclear fraction. SDS/polyacrylamide-gel electrophoresis, immunoblotting, and protein determination were carried out as previously described (11).

Relative Quantitation of rNQO1 and rNrf2 mRNA

This was carried out by TaqMan® chemistry. Total RNA was isolated from RL34 cells using Trizol reagent (Invitrogen). Approximately 1.5 μg of total RNA was reverse-transcribed to cDNA using random hexamers (Promega) and the SuperScript™ II RT kit (Invitrogen) according to the manufacturer's instructions.

For the real-time PCR analysis, the following matching oligonucleotide primers and probes, designed using PrimerExpress™ software (PerkinElmer Life Sciences), were used as follows: rNQO1, forward primer, 5′-GCAGGATTCGCCTACACGTATG-3′, and reverse primer, 5′-GGTGATGGAAAGCAAGGTCTTC-3′; Probe 5′-(6-carboxyfluorescein)CACCATGTATGACCAAGGTCCTTTCCAGAATA(6-carboxyl tetramethylrhodamine)-3′; rNrf2, forward primer, 5′-TTTGGCAGAGACATTCCCATT-3′, and reverse primer, 5′-GGGTGGTGAAGACTGAGCTCTCA-3′, Probe 5′-(6-carboxyfluorescein)AGATGACCATGAGTCGCTTGCCCT(6-carboxyl tetramethylrhodamine)-3′. The PCR mixes were prepared and amplified as described previously (16). The expression of 18 S rRNA was used as an internal control and was quantitated by TaqMan® chemistry using the TaqMan® ribosomal RNA control reagent (PerkinElmer Life Sciences).

Data acquisition and analysis utilized the ABI PRISM® 7700 sequence detection system (PerkinElmer Life Sciences). The relative gene expression levels in different samples was calculated using the Comparative C_T Method as outlined in the ABI PRISM® 7700 Sequence Detection System User Bulletin 2.

In Vivo Ubiquitination Assay

This was carried out using the method of Treier *et al.* (30). COS1 cells were transfected with pHisUb along with either pcDNA3.1/V5mNrf2 or pcDNA3.1/V5mNrf2$^{\Delta ETGE}$ and other expression vectors as described in Fig. 7. Approximately 24 h later, the transfected cells were treated with 10 μM MG132 for 2 h before the monolayers were washed with prewarmed phosphate-buffered saline and scraped into 0.36 ml of phosphate-buffered saline. A whole-cell lysate was prepared from 50 μl of the cell suspension and is referred to as the "input" fraction. His-tagged protein was purified from the remainder of the cell suspension as follows; the cell suspension was lysed by the addition to 2.2 ml of buffer A (6 M guanidine, 10 mM Tris, 0.1 M phosphate buffer, pH 8.0) supplemented with 5 mM imidazole. The resulting lysate was sonicated to reduce viscosity before 50 μl of Ni-CAM® HC resin (Sigma) was added, and the mixture was rotated overnight at 4 °C. Thereafter, the beads were washed sequentially with buffer A supplemented with 10 mM 2-mercaptoethanol (2-ME), buffer B (8 M urea, 10 mM Tris, 0.1 M phosphate buffer, pH 8.0) supplemented with 10 mM 2-ME, buffer C (8 M urea, 10 mM Tris, 0.1 M phosphate buffer, pH 6.3) supplemented with 10 mM 2-ME and 0.2% (v/v) Triton X-100, and finally, buffer C supplemented with 10 mM 2-ME and 0.1% (v/v) Triton X-100. Bound material was eluted from the beads by suspension in 50 μl of modified Laemmli sample buffer (20 mM Tris-Cl, pH 6.8, 10% (v/v) glycerol, 0.8% (w/v) SDS, 0.1% (w/v) bromphenol blue, 0.72 M 2-ME, and 300 mM imidazole) followed by boiling for 4 min. The suspension was centrifuged (16,000 × *g*, 1 min, 20 °C), and the resulting supernatant was collected and is referred to as the "pull-down" fraction.

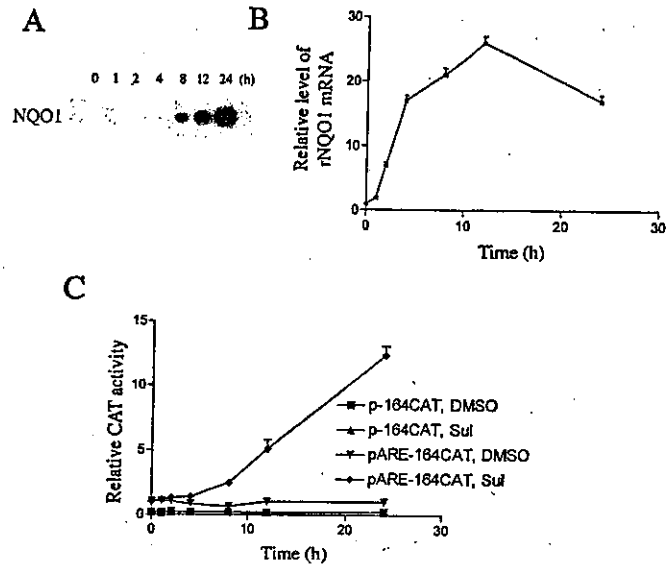

FIG. 1. **Sulforaphane causes transcriptional activation of rNQO1 in RL34 cells.** RL34 cells were treated with 15 μM Sul for the indicated periods of time and whole-cell lysates were immunoblotted with rabbit anti-rNQO1 (*A*) or total RNA was isolated from triplicate dishes (*B*), and the relative expression of rNQO1 mRNA was determined by real-time PCR using TaqMan® chemistry (mean ± S.D.). *C*, RL34 cells in 6-well plates were transfected with 0.4 μg of either pARE-164CAT or p-164CAT, 0.4 μg of pCMVβ-gal (internal control), and 1.2 μg of empty vector (pcDNA3.1/V5HisC). Cells in triplicate wells were treated with 15 μM Sul or vehicle (0.1% (v/v) dimethyl sulfoxide (*DMSO*) and lysed after the indicated periods of time. The CAT and β-galactosidase activities of each lysate were determined. The internally controlled and normalized CAT activity (mean ± S.D.) is depicted as a function of time.

RESULTS

Sulforaphane Transcriptionally Activates rNQO1 in RL34 Cells—Previous workers have shown that *NQO1* genes are regulated by agents that cause oxidative stress, and evidence suggests that this is mediated by Nrf2 through an ARE (11, 33, 34). In the present study, we sought to provide further information about how the function of Nrf2 is controlled by oxidative stress. To this end, the isothiocyanate Sul, which causes oxidative stress by reacting with GSH to form dithiocarbamates, (35), was chosen as the oxidative stressor. As a model system we chose the non-transformed rat RL34 cell line over the more commonly utilized human HepG2 and mouse Hepa1c1c7 cell lines because its phenotypic response to Sul more closely recapitulates that observed in rodent liver. Specifically, untreated RL34 cells express an undetectable level of rNQO1 protein that is highly inducible by Sul treatment (Fig. 1*A*). By contrast, HepG2 and Hepa1c1c7 cell lines both express high basal levels of NQO1 with little or no induction observed after treatment with Sul (data not shown). The accumulation of rNQO1 protein in the RL34 cell line is paralleled by a rapid (significantly increased after 1 h, $p < 0.05$) elevation in the level of its cognate mRNA (Fig. 1*B*). As CAT activity expressed from the pARE-164CAT construct, but not p-164CAT, is induced by Sul (Fig. 1*C*), the increase in NQO1 protein is a

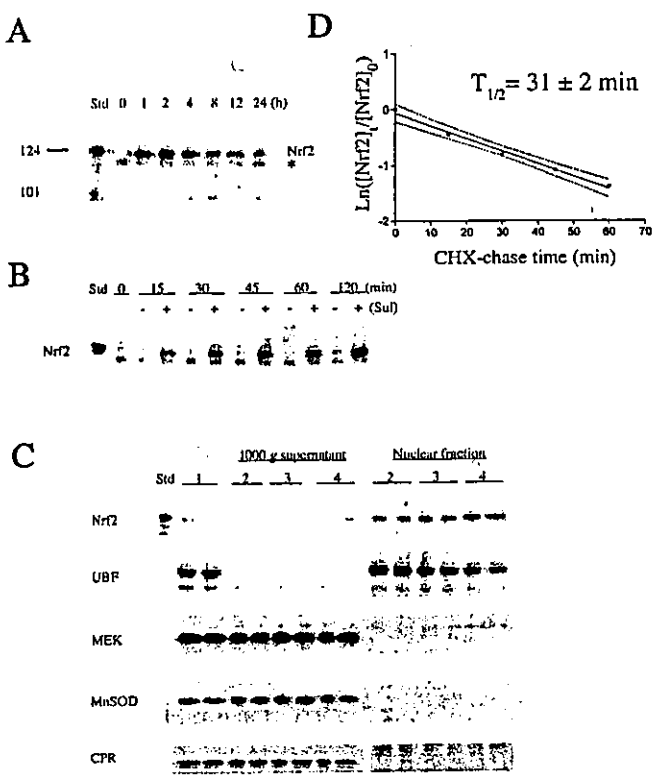

FIG. 2. **Sulforaphane causes rapid nuclear accumulation of rNrf2 in RL34 cells.** *A*, whole-cell lysates prepared from RL34 cells treated with 15 μM Sul for the indicated periods of time were electrophoresed through a 6% resolving gel and probed with rabbit anti-mNrf2. A 1.4-ng portion of immunogen was used as a standard. M_r markers are indicated to the *left* of the blot. A cross-reacting band, which comigrates with the rNrf2 band in 10% resolving gels, is indicated by an *asterisk*. *B*, whole-cell lysates were prepared from RL34 cells treated with 15 μM Sul (+) or vehicle (−) for the indicated periods of time and blotted with rabbit anti-mNrf2. *C*, whole-cell lysates were prepared from duplicate dishes of untreated RL34 cells (*lanes 1*). Nuclear and 1000 × *g* supernatant fractions were prepared from duplicate dishes of untreated RL34 cells (*lanes 2*) or cells treated for 2 h with vehicle (*lanes 3*) or 15 μM Sul (*lanes 4*). 16 μg (whole-cell lysates), 12 μg (1000 × *g* supernatant fractions), and 6 μg (nuclear fractions) of protein were separated through a 10% resolving gel and probed with antibodies raised against the proteins indicated on the *left*. The band developed by the anti-mNrf2 antiserum in nuclear fractions from untreated and vehicle-treated cells (nuclear fraction *lanes 2* and *3*) does not represent rNrf2, but the band indicated by an *asterisk* in *A*. *UBF*, upstream binding factor; *MnSOD*, manganese superoxide dismutase; *CPR*, cytochrome P450 reductase; *MEK*, mitogen-activated protein kinase-extracellular regulated kinase. *D*, RL34 cells were treated with 15 μM Sul for 2 h before the addition of CHX to a final concentration of 10 μM. Subsequently, whole-cell lysates were prepared at different time points and probed with rabbit anti-mNrf2. The graph depicts the natural logarithm of the relative expression of rNrf2 protein (quantitated by densitometry) as a function of CHX-chase time (mean ± S.D. of three independent experiments). The best-fit line, 95% confidence limits (*broken lines*), and the derived half-life ($t_{1/2}$) are presented.

consequence of transcriptional activation of *rNQO1* promoter, presumably mediated by Nrf2 through the ARE in the promoter of the oxidoreductase gene.

Sulforaphane Causes a Rapid Nuclear Accumulation of rNrf2 Protein—To determine how Sul controls rNrf2 activity in RL34 cells, whole-cell lysates were prepared at different times after Sul treatment and blotted with a rabbit anti-mNrf2 antiserum (Fig. 2*A*). An immunochemically cross-reacting electrophoretic band representing rNrf2 was identified by virtue of its comigration with the immunogen. Treatment of cells with Sul, but not vehicle, led to a rapid and sustained elevation in the level of this protein (Fig. 2, *A* and *B*). The Nrf2 protein could not be unequivocally identified in untreated RL34 cells but was readily detected 15 min after treatment with Sul. Its level

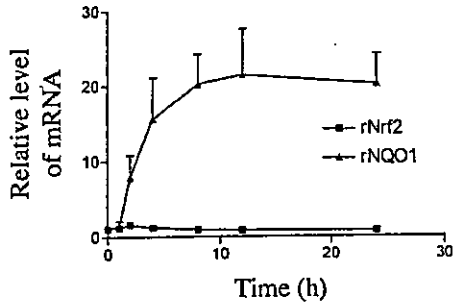

FIG. 3. **Sulforaphane does not increase expression of rNrf2 mRNA.** Total RNA was isolated from RL34 cells after treatment with 15 μM Sul for the indicated periods of time. The relative expression of rNrf2 and rNQO1 mRNA were determined by TaqMan® chemistry (mean ± S.D. of triplicate dishes).

appeared to peak between 2 and 4 h after Sul treatment and remained elevated for at least 24 h. Subcellular fractionation revealed that, whenever detectable, the majority of rNrf2 was associated with the nuclear fraction (Fig. 2*C*). The procedure provided a highly pure nuclear fraction with no evidence of cytoplasmic, mitochondrial, or endoplasmic reticulum contamination, as assessed by the absence of MEK (mitogen-activated protein kinase-extracellular regulated kinase), manganese superoxide dismutase, or cytochrome P450 reductase marker proteins, respectively.

Being undetectable in homeostatic RL34 cells, the stability of rNrf2 under such conditions remains a matter of conjecture. CHX-chase experiments revealed, however, that after 2 h of Sul treatment, degradation of rNrf2 followed first-order kinetics with an approximate half-life of 30 min (Fig. 2*D*).

Sulforaphane Antagonizes Proteasome-dependent Degradation of rNrf2—The amount of protein expressed in mammalian cells is controlled primarily by regulating its rate of degradation and/or by altering the transcriptional activation of its gene. Evidence that *Nrf2* might be transcriptionally activated by oxidative stress was presented by Kwak *et al.* (22, 23). Although such a mechanism could play some role in the later response to Sul, it is unlikely to account for the large increase in Nrf2 protein within the first 2 h. To discount the possibility that induction of *rNrf2* contributes to the accumulation of Nrf2 protein, we measured the level of mRNA for the protein after exposure of RL34 cells to Sul. Real-time PCR showed no statistically significant change in the expression of rNrf2 mRNA at any time. By contrast, rNQO1 mRNA levels were elevated 20-fold within 8 h (Fig. 3). We therefore conclude that Sul does not cause any significant transcriptional activation of *rNrf2*.

Failure of Sul to affect induction of rNrf2 mRNA suggested that the increase in rNrf2 protein observed after treatment with the isothiocyanate might be wholly due to a reduction in its rate of degradation. In eukaryotic cells, regulatable proteolysis of intracellular proteins is in most cases accomplished by the proteasome (36–38). The notion that Nrf2 protein levels might be controlled by Sul through a proteasome-based mechanism is supported by the work of Sekhar *et al.* (39) who reported that proteasome inhibition activated ARE-driven gene expression in HepG2 cells. More recently, it has been reported that *tert*-butylhydroquinone can stabilize hNrf2 in HepG2 cells, and $CdCl_2$ can stabilize mNrf2 protein in Hepa cells (24, 25). To evaluate the role of the proteasome in regulation of rNrf2, we treated RL34 cells with three structurally dissimilar proteasome inhibitors, epoxomicin, *clasto*-lactacystin-β-lactone (Fig. 4*A*), and MG132 (data not shown). All resulted in the accumulation of rNrf2, demonstrating that it is subject to proteasome-dependent degradation. In fact, after MG132-treatment of RL34 cells, CHX-chase experiments failed to reveal any

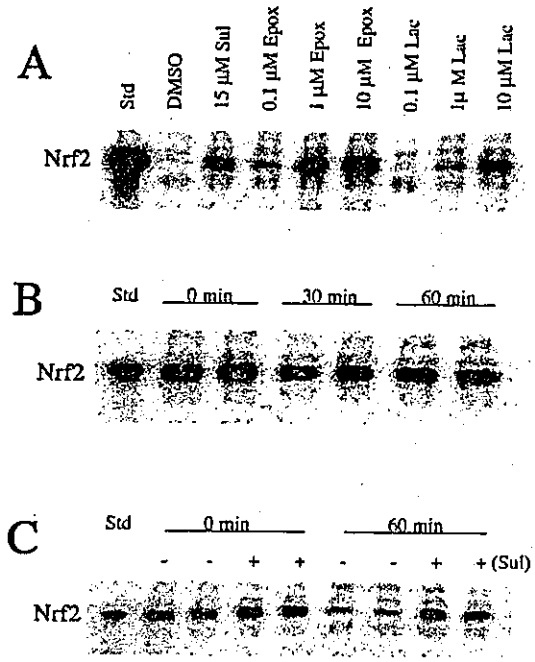

FIG. 4. **Sulforaphane stabilizes rNrf2 protein by antagonizing its proteasome-dependent degradation.** *A*, RL34 cells were treated with the indicated compounds for 2 h. Whole-cell lysates were prepared and immunoblotted with rabbit anti-mNrf2. A 1.4-ng portion of immunogen was used as standard. *B*, RL34 cells were cultured with 2.5 μM MG132 for 2 h before CHX was added to a final concentration of 10 μM. Whole-cell lysates were prepared from duplicate dishes 0, 30, and 60 min after the addition of CHX and probed with rabbit anti-mNrf2. *C*, RL34 cells were cultured with 2.5 μM MG132 for 2 h. Medium was removed, and all monolayers were washed with one volume of fresh medium. Fresh medium containing 10 μM CHX and either 15 μM Sul (+) or vehicle (−) was added to each dish. Whole-cell lysates were prepared from duplicate dishes 0 or 60 min later and were probed with rabbit anti-mNrf2. *DMSO*, Me_2SO; *Epox*, epoxomicin; *Lac*, *clasto*-lactacystin-β-lactone.

degradation of rNrf2 during a chase period of 60 min (Fig. 4*B*). This finding suggested that the major proteolytic activities responsible for rNrf2 degradation are proteasomal in nature. In addition, because rNrf2 was calculated to have a half-life of 31 min in Sul-treated cells (Fig. 2*D*), the bZIP protein appears to be subject to proteasome-mediated degradation even during oxidative stress.

Because rNrf2 protein cannot be unequivocally identified in homeostatic RL34 cells, we could not determine directly whether under such circumstances it is subject to a greater rate of proteasome-dependent degradation than when treated with Sul. To investigate this point, the fact that MG132-mediated inhibition of the proteasome is reversible was exploited to generate a measurable pool of rNrf2 in RL34 cells before either returning them to normal conditions or subjecting them to oxidative stress. RL34 cells were pretreated with MG132 for 2 h before the proteasome inhibitor was removed and replaced with media containing CHX and either Sul or vehicle. When cotreated with CHX and vehicle, a notable reduction in the expression of rNrf2 was observed after a chase period of 60 min (Fig. 4*C*), indicative of proteasomal-mediated degradation. Most importantly, this degradation was clearly inhibited by cotreatment with Sul. Overall, these data suggest that Nrf2 is subject to proteasome-dependent degradation under both homeostatic and oxidative stress conditions but that the rate of degradation is reduced significantly during oxidative stress. Redox-regulated proteasomal degradation is likely to be a universal feature of Nrf2 regulation, at least in mammals.

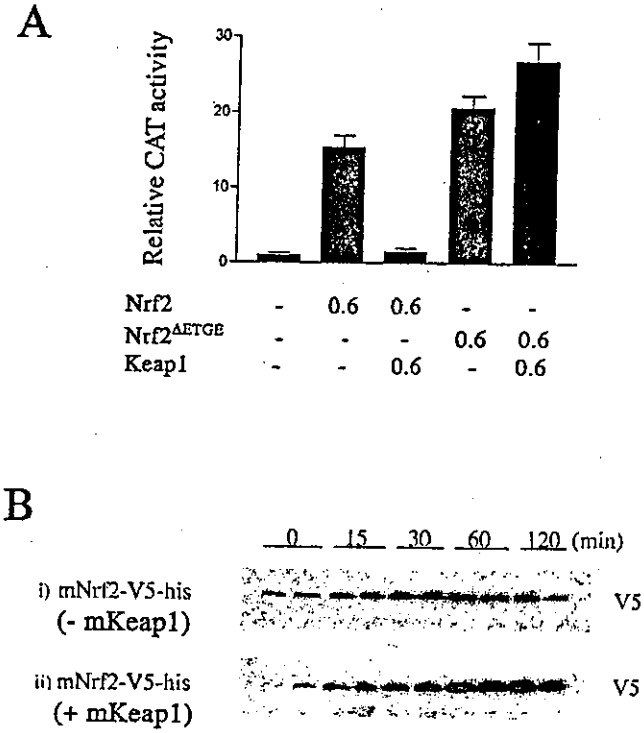

FIG. 5. **Keap1 confers redox-sensitivity upon the level of Nrf2.** *A*, COS1 cells in 6-well plates were cotransfected with 0.4 μg of pARE-164CAT reporter vector, 0.4 μg of pCMVβ-gal, and the indicated amounts of the following expression plasmids: Nrf2, pcDNA3.1/V5HisBmNrf2; $Nrf2^{\Delta ETGE}$, pcDNA3.1/V5HisBm$Nrf2^{\Delta ETGE}$; Keap1, pcDNA3.1/V5HisCmKeap1. All transfection mixes were made up to 2 μg of total plasmid with pcDNA3.1/V5HisC. After transfection (24 h), whole-cell lysates were prepared, and the CAT and β-galactosidase activities were determined. The relative CAT activities are depicted (mean ± S.D. of three independent experiments.) *B*, COS1 cells in 60-mm dishes were cotransfected with 2 μg of pcDNA3.1/V5HisBmNrf2, 0.8 μg of pCMVβ-gal, and either 2 μg of pcDNA3.1/V5HisC (*i*) or 2 μg of pcDNA3.1/mKeap1 (*ii*). After 24 h, dishes were treated with 15 μM sulforaphane, and whole-cell lysates were prepared from duplicate dishes at the indicated time points. The β-galactosidase activity of each lysate was determined. Volumes of lysate containing equivalent amounts of β-galactosidase activity were electrophoresed through an 8% resolving gel and blotted with mouse anti-V5.

Direct Interaction between Keap1 and Nrf2 Is Essential to Confer Oxidative Stress Dependence on the Level of Nrf2—To explore the mechanism underlying the oxidative stress-regulated degradation of Nrf2, we sought to reconstitute this phenotype in COS1 cells by heterologously expressing epitope-tagged Nrf2 along with untagged Keap1. In COS1 cells, ectopic expression of mNrf2-V5-his induced ARE-driven CAT activity, which was suppressed by coexpression of mKeap1, whereas transactivation of the reporter construct by heterologous expression of $mNrf2^{\Delta ETGE}$-V5-his, a mutant Nrf2 which lacks the tetrapeptide motif between amino acids 79 and 82 essential for the Nrf2/Keap1 interaction, was not ablated by coexpression of mKeap1 (Fig. 5*A*).

When pcDNA3.1/V5hisBmNrf2 was transfected alone into COS1 cells, the level of mNrf2-V5-his protein was only minimally responsive to the applied oxidative stress (Fig. 5*B*, *panel i*). Coexpression of mNrf2-V5-his and mKeap1 was required to confer significant oxidative stress dependence upon the level of the bZIP protein (Fig. 5*B*, *panel ii*), an affect that appeared to result solely from a diminution in the level of the transcription factor under homeostatic conditions when coexpressed with mKeap1. The data in Fig. 5, *panel ii*, might suggest that mNrf2-V5-his protein is expressed at higher levels in the presence of mKeap1 than without mKeap1 after sulforaphane

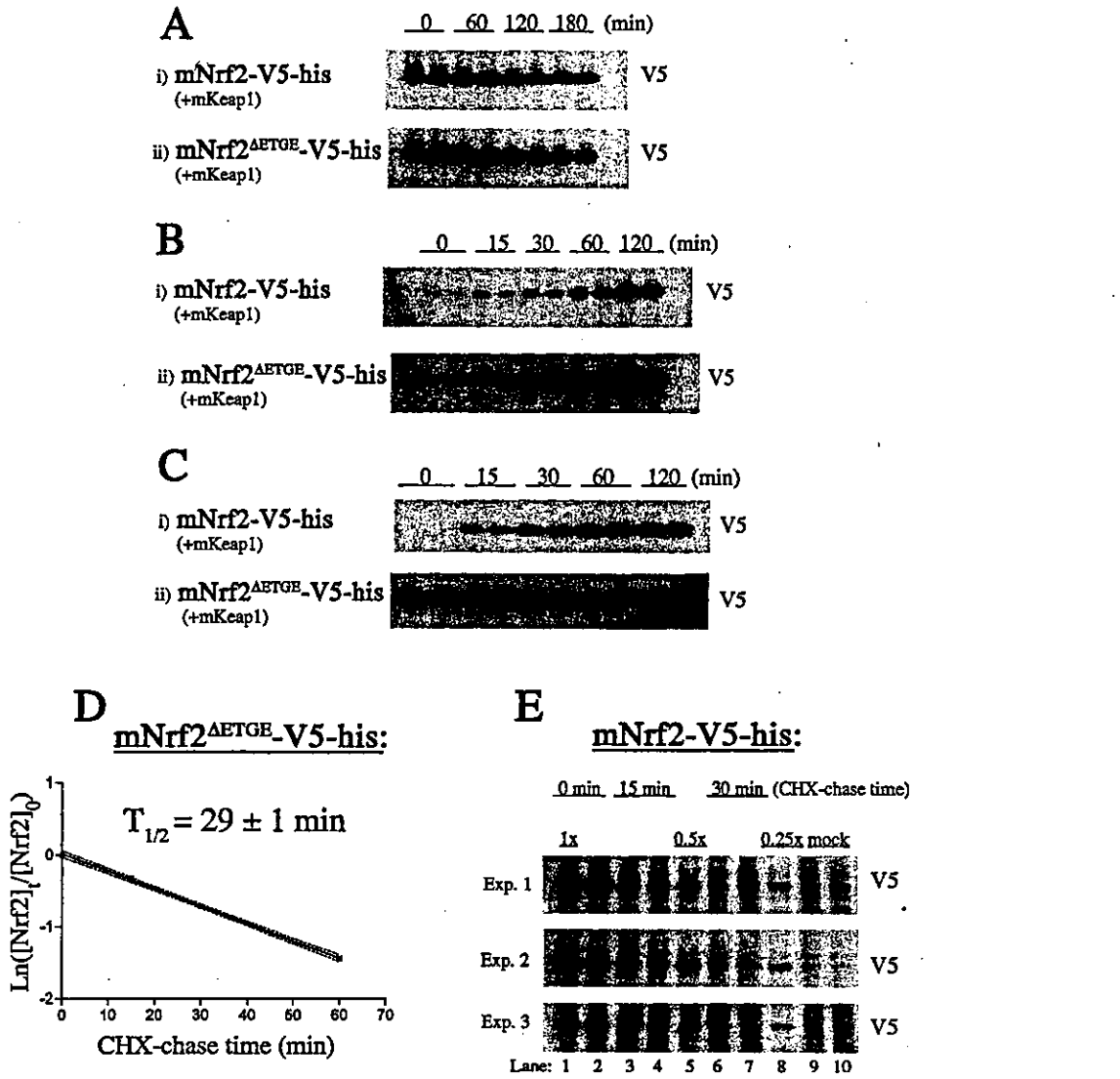

FIG. 6. **Keap1 destabilizes Nrf2 by directly interacting with it.** *A*, COS1 cells were transfected with 2 μg of pcDNA3.1/mKeap1, 0.8 μg of pCMVβ-gal, and either 2 μg of pcDNA3.1/V5HisBmNrf2 (*i*) or 2 μg of pcDNA3.1/V5HisBmNrf2$^{\Delta ETGE}$ (*ii*). After 24 h, cells were treated with 10 μM MG132 for 2 h before CHX was added to a final concentration of 10 μM. Whole-cell lysates were prepared from duplicate dishes at the indicated time points and blotted with mouse anti-V5. *B* and *C*, COS1 cells were transfected as described for *A*, and cells were treated with either 10 μM MG132 (*B*) or 15 μM Sul (*C*) for the indicated periods of time before whole-cell lysates were prepared from duplicate dishes and blotted with mouse anti-V5. *D*, COS1 cells were cotransfected with 2 μg of pcDNA3.1/V5HisBmNrf2$^{\Delta ETGE}$, 2 μg of pcDNA3.1/mKeap1, and 0.8 μg of pCMVβ-gal. After transfection (24 h), CHX was added to each culture to a final concentration 10 μM, and whole-cell lysates were prepared from duplicate dishes of cells at different CHX-chase times and probed with anti-V5. The *graph* depicts the natural logarithm of the relative expression (quantitated by densitometry) of mNrf2$^{\Delta ETGE}$-V5-his as a function of the CHX-chase time (mean ± S.D. of three independent experiments). *E*, COS1 cells were cotransfected with 2 μg of pcDNA3.1/V5HisBmNrf2, 2 μg of pcDNA3.1/mKeap1, and 0.8 μg of pCMVβ-gal. Later (24 h after transfection), CHX was added to a final concentration of 10 μM, and whole-cell lysates were prepared after the indicated CHX-chase periods. Equal volumes of lysates were electrophoresed through an 8% gel and blotted with anti-V5. 0.5 volume (*lane 5*) and 0.25 volume (*lane 8*) of the CHX-chase sample obtained at 0 min (*lane 1*) were also included to allow estimation of the amount of mNrf2-V5-his remaining at each time point. Whole-cell lysates were also prepared from duplicate dishes of mock-transfected cells and run in *lanes 9* and *10*. The low signal-to-noise ratio did not allow densitometric scanning of the three blots (from three independent experiments) depicted. Nevertheless, it is clear that in each case, a CHX-chase period of between 7.5 and 15 min reduced the amount of mNrf2-V5-his by half.

treatment for 60 and 120 min. This interpretation is incorrect, and the difference in the mNrf2-V5-his signal merely results from the fact that the protein was blotted onto two different membranes (albeit at the same time). No experimental evidence has been obtained to support a difference in the expression of mNrf2-V5-his after 2 h of sulforaphane treatment regardless of the presence or absence of coexpressed mKeap1 (data not shown).

The above findings suggest that under homeostatic conditions Keap1 increases the rate of proteasomal degradation of Nrf2 through a direct interaction and that during oxidative stress this interaction is antagonized, exposing Nrf2 to a reduced rate of proteasomal degradation. To test this model we compared the biological properties of mNrf2-V5-his coexpressed with mKeap1 with the mutant Nrf2, mNrf2$^{\Delta ETGE}$-V5-his, coexpressed with mKeap1. Mutant mNrf2$^{\Delta ETGE}$-V5-his was found to be subject to proteasomal degradation, judged by the fact its half-life in homeostatic COS1 cells was 29 min (Fig. 6*D*), but when treated with MG132, its half-life increased to at least 3 h (Fig. 6*A*, *panel ii*). Thus, mutant Nrf2 protein accumulated in response to treatment with MG132 (Fig. 6*B*, *panel ii*). As predicted by the model, the level of mNrf2$^{\Delta ETGE}$-V5-his protein, which could not interact with mKeap1, was not influenced by treatment with Sul (Fig. 6*C*, *panel ii*), indicating that its half-life is independent of the redox environment. mNrf2-V5-his was also subject to proteasomal degradation (Fig. 6*A*,

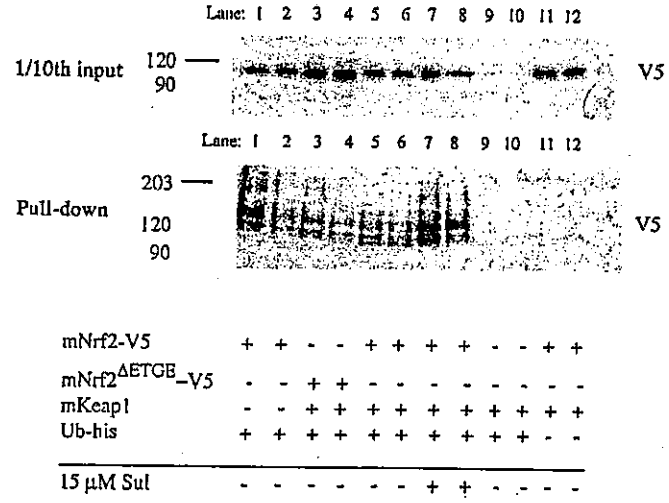

FIG. 7. **Nrf2 is ubiquitinated in a Keap1- and oxidative stress-independent fashion.** Duplicate dishes of COS1 cells were transfected with the indicated plasmids. After transfection (24 h), cells were treated with 10 μM MG132 for 2 h with or without cotreatment with 15 μM Sul before both a whole-cell lysate (*input*) and affinity-purified His-tagged protein fraction (*Pull-down*) were prepared from each dish of transfected cells and blotted with anti-V5. M_r markers are indicated to the *left* of each blot.

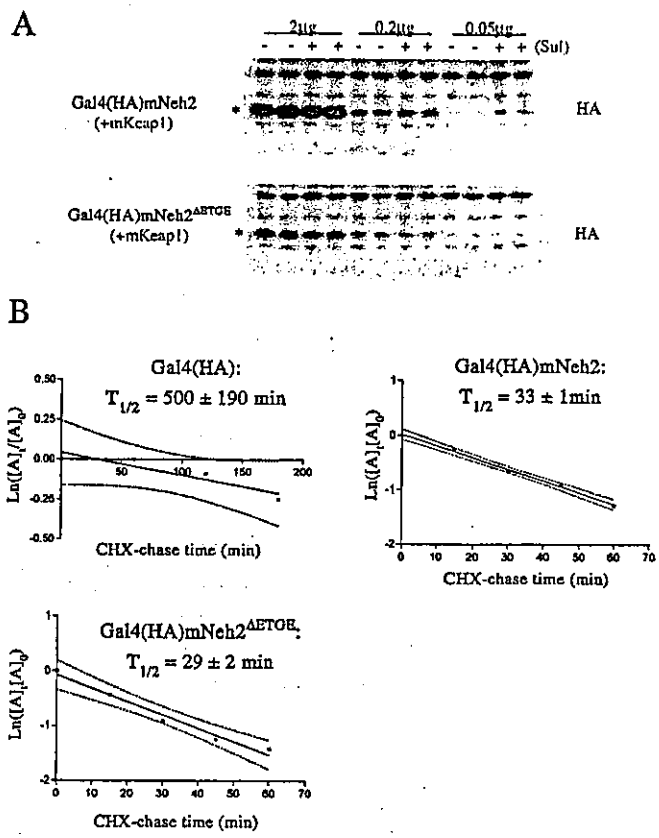

FIG. 8. **The Neh2 domain of Nrf2 constitutes a redox-sensitive degron.** *A*, COS1 cells were transfected with 2 μg of pcDNA3.1/mKeap1, 0.8 μg of pCMVβ-gal, and the indicated amounts of either pCG-GAL(HA)mNeh2 or pCG-GAL(HA)mNeh2$^{\Delta ETGE}$. All transfection mixes were made up to the same amount of DNA with pcDNA3.1/V5HisC. After 24 h, duplicate dishes of cells were treated with either 15 μM Sul (+) or vehicle (-) for 2 h, and whole-cell lysates were prepared and blotted with anti-HA. The bands representing the fusion proteins are shown with an *asterisk*. *B*, COS1 cells were cotransfected with 2 μg of pcDNA3.1/mKeap1, 0.8 μg of pCMVβ-gal, and 2 μg of either pCG-GAL(HA), pCG-GAL(HA)mNeh2, or pCG-GAL(HA)mNeh2$^{\Delta ETGE}$. Twenty-four h after transfection, CHX was added to a final concentration of 10 μM, and whole-cell lysates were prepared from duplicate dishes of cells after the indicated CHX-chase periods and probed with anti-HA. The *graphs* depict the natural logarithm of the relative expression (quantitated by densitometry) of the indicated proteins as a function of the CHX-chase time (mean ± S.D. of three independent experiments).

panel i, and *B*, *panel i*), but two major differences were observed between it and mNrf2$^{\Delta ETGE}$-V5-his. First, under homeostatic conditions mNrf2-V5-his was less stable than mNrf2$^{\Delta ETGE}$-V5-his. Although we could not model precisely its kinetics of degradation, a CHX-chase period of between 7.5 and 15 min was sufficient to reduce mNrf2-V5-his expression by half (Fig. 6*E*). This compares with a half-life of 29 min for mNrf2$^{\Delta ETGE}$-V5-his (Fig. 6*D*). Not surprisingly therefore, mNrf2-V5-his was present at lower levels than was the mutant protein under homeostatic conditions (Fig. 6*C*). Second, mNrf2-V5-his was found to accumulate rapidly in COS1 cells after exposure to Sul, demonstrating that its half-life was increased by oxidative stress (Fig. 6*C*). As a consequence, the level of wild-type Nrf2 protein approached that of mutant Nrf2 protein after Sul-treatment.

These results demonstrate that Nrf2 is subject to at least two different modes of proteolysis. First, there exists a Keap1-independent, redox-insensitive proteasomal degradation responsible for the short half-life of rNrf2 in oxidatively stressed RL34 cells (31 min) and for the half-life of mNrf2$^{\Delta ETGE}$-V5-his in COS1 cells (29 min). Second, Nrf2 is subject to a substantially more rapid Keap1-dependent, redox-dependent proteasomal degradation. Thus, Keap1 appears to function as a *trans*-acting factor that stimulates the rate of proteasomal degradation of Nrf2. This activity entails a physical interaction between Keap1 and Nrf2 that occurs under homeostatic conditions but not during oxidative stress (18).

Nrf2 Is Ubiquitinated in Vivo in a Keap1- and Redox-independent Fashion—Many substrates of the 26 S proteasome require polyubiquitination to target them for degradation (40). In light of the data in Fig. 6, we were interested in determining whether Nrf2 is subject to ubiquitination and, if so, whether the ubiquitination is modulated by Keap1 and/or Sul treatment. To determine the ubiquitination status of Nrf2, COS1 cells were transfected with vectors expressing the proteins indicated in Fig. 7. After 24 h, cells were treated with MG132 with or without Sul cotreatment as indicated. Subsequently, His-tagged proteins were affinity-purified and assayed for the presence of V5-tagged proteins by immunoblot analysis (Fig. 7). A smear of high molecular mass V5-tagged protein was evident in the "pull-down" fraction of COS1 cells cotransfected with mNrf2-V5, mKeap1, and Ub-his (*lanes 5* and *6*). Because no V5-tagged protein was detected if the vector expressing either mNrf2-V5 (*lanes 9* and *10*) or Ub-his (*lanes 11* and *12*) was omitted from the transfection, this smear represents polyubiquitinated mNrf2-V5. In addition, Fig. 7 also demonstrated that polyubiquitination of Nrf2 occurs in a Keap1-independent fashion; in the absence of heterologously expressed mKeap1, mNrf2-V5 was still ubiquitinated (*lanes 1* and *2*), and heterologously expressed mNrf2$^{\Delta ETGE}$-V5 (*lanes 3* and *4*) was successfully polyubiquitinated in this assay. Finally, oxidative stress caused by treatment with Sul did not impair the ubiquitination of mNrf2-V5 (compare *lanes 5* and *6* with *lanes 7* and *8*). It is, therefore, concluded that Nrf2 can be ubiquitinated by a mechanism that is independent of both Keap1 and the redox environment of the cell.

The Neh2 Domain of Nrf2 Constitutes a Redox-sensitive Degron—Although it was evident that the ETGE tetrapeptide motif of Nrf2 is essential for its Keap1-dependent degradation, it was unclear what *cis*-acting sequences within the transcription factor were sufficient to target it for redox-sensitive degradation by the proteasome. We postulated that its Neh2 do-

main, which is highly conserved across species and contains the ETGE tetrapeptide motif, might serve as a redox-sensitive "degron" (a protein sequence sufficient to confer metabolic instability; see Varshavsky (41)). To evaluate this hypothesis, constructs expressing either the mNeh2 domain or mNeh2$^{\Delta ETGE}$ fused to the C terminus of a HA-tagged GAL4 DNA binding domain were generated.

An initial experiment revealed that during heterologous coexpression of either GAL4(HA)mNeh2 or GAL4(HA) mNeh2$^{\Delta ETGE}$ with mKeap1, the level of neither fusion protein was altered when the COS1 cells were exposed to Sul (data not shown). One explanation considered for the failure of mKeap1 to confer redox sensitivity upon the expression level of Gal4(HA)mNeh2 protein was that the level of expression of the N-terminal fusion protein might be sufficiently great as to saturate the binding capacity of the heterologously expressed mKeap1. To reduce the expressed levels of these fusion proteins, we transfected reduced amounts of the relevant expression constructs into COS1 cells. In line with the above interpretation, when lower amounts of the fusion proteins were expressed, the expression of GAL4(HA)mNeh2 became Sul-dependent, in contrast to the expression of GAL4(HA) mNeh2$^{\Delta ETGE}$ (Fig. 8*A*). Next, we sought to show that the half-life of the HA-tagged GAL4 DNA binding domain was reduced by fusing the mNeh2 domain to its C terminus. Because of a low signal-to-noise ratio, it was not possible to calculate or estimate by immunoblot analysis the half-life of Gal4(HA) mNeh2 or GAL4(HA)mNeh2$^{\Delta ETGE}$ when they were expressed at the low levels required to confer redox sensitivity upon the expression level of the wild-type fusion protein. Nonetheless, when expressed at higher levels, CHX-chase experiments revealed that the half-lives of both GAL4(HA)mNeh2 (33 min) and GAL4(HA)mNeh2$^{\Delta ETGE}$ (29 min) were much shorter than that of GAL4(HA) (500 min) (Fig. 8*B*). The similar half-life of both fusion proteins is in complete accordance with the observation that, under these transfection conditions, the expression of Gal4(HA)mNeh2 protein was unaltered by sulforaphane treatment. The calculated half-lives for both fusion proteins are close to those calculated for mNrf2$^{\Delta ETGE}$-V5-his in COS1 cells (Fig. 6*D*), suggesting that the Neh2 domain of Nrf2 is the sole *cis*-acting determinant of Nrf2 stability. Overall, these data suggest that the Neh2 region of Nrf2 constitutes a redox-sensitive degron.

DISCUSSION

This paper contains the first report that Nrf2 is subject to constitutive, Keap1-independent polyubiquitination and degradation by the proteasome. During oxidative stress, this appears to be the sole mechanism accounting for degradation of the bZIP transcription factor. It confers a half-life of 31 min upon rNrf2 in oxidatively stressed RL34 cells and a half-life of 29 min upon mNrf2$^{\Delta ETGE}$-V5-his heterologously expressed in COS1 cells (*cf.* Figs. 2*D* and 6*D*). The ubiquitin-conjugating enzymes involved in the process remain unidentified, but the Neh2 domain of Nrf2 constitutes the relevant degron.

Under homeostatic conditions, the amount of Nrf2 protein in the RL34 cell line (this paper), other cell lines (23–25), and in murine liver (22) is significantly lower than in cells subjected to oxidative stress. This reduction is a consequence of a second more rapid mode of proteasomal degradation of Nrf2 that operates in non-stressed cells and requires Keap1 as an essential *trans*-acting factor (Figs. 5 and 6). Keap1 increases the homeostatic rate of proteasomal degradation of Nrf2 by directly interacting with it via the ETGE tetrapeptide motif present between residues 79 and 82 in the Neh2 domain of the bZIP protein (Figs. 5 and 6). The fact that this interaction is antagonized by oxidative stress (19) explains why this mode of degradation is restricted to homeostatic conditions. The half-life of endogenous rNrf2 in non-stressed RL34 cells could not be calculated because it was undetectable, but the half-life of mNrf2-V5-his heterologously coexpressed with mKeap1 in homeostatic COS1 cells was between 7.5 and 15 min. By contrast, the half-life of mNrf2$^{\Delta ETGE}$-V5-his heterologously expressed under the same conditions was ~30 min (Fig. 6).

Although the Neh2 domain of Nrf2 constitutes a degron common to both Keap1-independent and -dependent degradation of Nrf2 (Fig. 8), the mechanism of Keap1-dependent degradation and its relationship to Keap1-independent degradation remains a matter of conjecture. It is not known whether the Keap1-dependent degradation of Nrf2 involves a direct enhancement of the Keap1-independent degradation or constitutes a distinct parallel pathway. It is not even clear whether the Keap1-dependent pathway requires polyubiquitination of Nrf2. In yeast, the efficient degradation of many proteins, such as Matα2 and Far1, requires their localization to discrete cellular compartments, apparently due to the non-uniform distribution of components of the ubiquitin system and the proteasome (42, 43). In mammalian cells, the proteasome and ubiquitin-conjugating enzymes also appear to be non-uniformly distributed throughout the cytoplasm and the nucleus (38, 44–46). In common with many other Kelch-repeat proteins (for review, see Ref. 47), Keap1 has a restricted cellular distribution, being localized to the cytoskeleton (19, 48, 49). Thus, Keap1 may recruit Nrf2 in a redox-dependent manner to regions of the cytoskeleton to facilitate proteasomal degradation. Certainly, proteasomes have been observed localized to the cytoskeleton in mammalian cells (Ref. 45 and references therein). It is even possible that Keap1 might actively recruit Nrf2 to the proteasome, a notion supported by the functional similarity between Keap1 and the recently identified yeast protein Cic1 (50). Like Keap1, Cic1 increases the rate of proteasomal degradation of specific substrates (the SCF subunits Cdc4 and Grr1) but has no effect on the global rate of proteasomal degradation. Cic1 was originally isolated in a yeast two-hybrid screen for proteins interacting with the α4 subunit of the yeast proteasome and appears to act as an adaptor between the relevant SCF complexes and the proteasome, thereby ensuring the preferential proteasomal degradation of important regulatory proteins over the general population of ubiquitinated substrates (50). The existence in mammalian cells of proteins with characteristic similar to Cic1 or "extrinsic factors that assist in the recognition of certain substrates" (40), has been predicted. Keap1 may act as such a factor by a similar mechanism to that observed for Cic1. Keap1 appears to function as a dimer (49), with each monomer containing six Kelch-repeat motifs (19). Because this motif represents a general protein-protein interaction module (47), Keap1 possesses the characteristics required to bind and bring together multiple proteins.

It is curious that reports to date on Keap1 function have emphasized its sequestration of Nrf2 in the cytosol without noting an enhanced rate of degradation of Nrf2 (19, 48). It should be borne in mind that although heterologous expression of Nrf2 and Keap1 in cells is sufficient to observe an interaction between the two proteins, enhanced degradation of Nrf2 might require other conditions to be fulfilled. Thus, we have shown that Keap1 is essential to enhance the rate of degradation of Nrf2 in homeostatic cells but have not demonstrated that it is sufficient for this purpose. It is likely that the consequence of the Keap1-Nrf2 interaction will depend upon the amounts of heterologous proteins expressed and the cell line studied. It is intriguing to note that mouse liver (22) and two non-transformed cell lines (RL34 (this study) and PE cells (23)) contain no detectable Nrf2 protein under homeostatic conditions. By

contrast, two of three transformed cell lines for which data are available (HepG2 and H4IIEC3 (24)) contain detectable levels of Nrf2 proteins under homeostatic conditions, and treatment of these cell lines with oxidative stressors only modestly increases the half-lives and levels of the bZIP proteins. It has been argued that up-regulation of GSH-dependent enzymes might contribute to the transformed phenotype by allowing cancerous cells to better withstand oxidative stress (51, 52), and it is conceivable that in certain transformed cell lines Keap1 function is partly disabled, and it does not efficiently degrade Nrf2. This might be one explanation for the high expression of NQO1 in HepG2 cells. In cell lines emphasizing the sequestration of heterologously expressed Nrf2 by heterologously expressed Keap1, not only might Nrf2 not be destabilized by Keap1, but rather, by competing with the endogenous ubiquitin ligases for Nrf2, Keap1 might actually stabilize Nrf2, as has been observed in HepG2 cells by Sekhar *et al.* (53).

In conclusion, the half-life of Nrf2 is coupled to the redox state of the cell by means of a redox-sensitive interaction between the ETGE tetrapeptide motif of its Neh2 degron and Keap1, a cytoskeleton-bound protein. This interaction does not occur in oxidative-stressed cells, and under these conditions, Nrf2 is subject to Keap1-independent ubiquitination and proteasome-mediated degradation. However, in homeostatic cells Keap1 binds Nrf2 and by doing so substantially reduces the half-life of the transcription factor from that observed in oxidative-stressed cells. This redox-sensitive half-life enables rapid accumulation of total cellular levels of Nrf2 in response to oxidative stress, which contributes to the increase in nuclear levels of the transcription factor, the induction of cytoprotective genes, and ultimately, the restoration of homeostasis. In turn, this destabilizes Nrf2, and the adaptive response is switched off. How the redox environment of the cell is linked to the Keap1-Nrf2 interaction and how Keap1 enhances the rate of degradation of Nrf2 are subjects worthy of further inquiry.

Acknowledgments—We thank Dr. Brian McStay, Dr. William Tansey, Prof. David Lane, Dr. Sonia Lain, and Dr. Sam Crouch for expert advice and help.

REFERENCES

1. Schafer, F. Q., and Buettner, G. R. (2001) *Free Radic. Biol. Med.* **30**, 1191–1212
2. Cadenas, E. (1995) in *Oxidative Stress and Antioxidant Defenses in Biology* (Ahmad, S., ed) pp. 1–61, Chapman & Hall, New York
3. Dalton, T. P., Shertzer, H. G., and Puga, A. (1999) *Annu. Rev. Pharmacol. Toxicol.* **39**, 67–101
4. Inamdar, N. M., Ahn, Y. I., and Alam, J. (1996) *Biochem. Biophys. Res. Commun.* **221**, 570–576
5. Moinova, H. R., and Mulcahy, R. T. (1999) *Biochem. Biophys. Res. Commun.* **261**, 661–668
6. Ishii, T., Itoh, K., Takahashi, S., Sato, H., Yanagawa, T., Katoh, K., Bannai, S., and Yamamoto, M. (2000) *J. Biol. Chem.* **275**, 16023–16029
7. Kim, Y-C., Masutani, H., Yamaguchi, Y., Itoh, K., Yamamoto, M., and Yodoi, J. (2001) *J. Biol. Chem.* **276**, 18399–18406
8. Li, J., Lee, J.-M., and Johnson, J. A. (2002) *J. Biol. Chem.* **277**, 388–394
9. Sasaki, H., Sato, H., Kuriyama-Matsumura, K., Sato, K., Maebara, K., Wang, H., Tamba, M., Itoh, K., Yamamoto, M., and Bannai, S. (2002) *J. Biol. Chem.* **277**, 44765–44771
10. Kelly, V. P., Ellis, E. M., Manson, M. M., Chanas, S. A., Moffat, G. J., McLeod, R., Judah, D. J., Neal, G. E., and Hayes, J. D. (2000) *Cancer Res.* **60**, 957–969
11. McMahon, M., Itoh, K., Yamamoto, M., Chanas, S. A., Henderson, C. J., McLellan, L. I., Wolf, C. R., Cavin, C., and Hayes, J. D. (2001) *Cancer Res.* **61**, 3299–3307
12. Thimmulappa, R. K., Mai, K. H., Srisuma, S., Kensler, T. W., Yamamoto, M., and Biswal, S. (2002) *Cancer Res.* **62**, 5196–5203
13. Nguyen, T., Sherratt, P. J., and Pickett, C. B. (2003) *Annu. Rev. Pharmacol. Toxicol.* **43**, 233–260
14. Motohashi, H., O'Connor, T., Katsuoka, F., Engel, J. D., and Yamamoto, M. (2002) *Gene (Amst.)* **294**, 1–12
15. Itoh, K., Chiba, T., Takahashi, S., Ishii, T., Igarashi, K., Katoh, Y., Oyake, T., Hayashi, N., Satoh, K., Hayatama, I., Yamamoto, M., and Nabeshima, Y.-I. (1997) *Biochem. Biophys. Res. Commun.* **236**, 313–322
16. Chanas, S. A., Jiang, Q., McMahon, M., McWalter, G. K., McLellan, L. I., Elcombe, C. R., Henderson, C. J., Wolf, C. R., Moffat, G. J., Itoh, K., Yamamoto, M., and Hayes, J. D. (2002) *Biochem. J.* **365**, 405–416
17. Kobayashi, M., Itoh, K., Suzuki, T., Osanai, H., Nishikawa, K., Katoh, Y., Takagi, Y., and Yamamoto, M. (2002) *Genes Cells* **7**, 807–820
18. Katoh, Y., Itoh, K., Yoshida, E., Miyagashi, M., Fukamizu, A., and Yamamoto, M. (2001) *Genes Cells* **6**, 857–868
19. Itoh, K., Wakabayashi, N., Katoh, Y., Ishii, T., Igarashi, K., Engel, J. D., and Yamamoto, M. (1999) *Genes Dev.* **13**, 76–86
20. Dinkova-Kostova, A. T., Holtzclaw, W. D., Cole, R. N., Itoh, K., Wakabayashi, N., Katoh, Y., Yamamoto, M., and Talalay, P. (2002) *Proc. Natl. Acad. Sci. U. S. A.* **99**, 11908–11913
21. Huang, H.-C., Nguyen, T., and Pickett, C. B. (2002) *J. Biol. Chem.* **277**, 42769–42774
22. Kwak, M.-K., Itoh, K., Yamamoto, M., Sutter, T. R., and Kensler, T. W. (2001) *Mol. Med.* **7**, 135–145
23. Kwak, M.-K., Itoh, K., Yamamoto, M., and Kensler, T. W. (2002) *Mol. Cell. Biol.* **22**, 2883–2892
24. Nguyen, T., Sherratt, P. J., Huang, H.-C., Yang, C. S., and Pickett, C. B. (2003) *J. Biol. Chem.* **278**, 4536–4541
25. Stewart, D., Killeen, E., Naquin, R., Alam, S., and Alam, J. (2003) *J. Biol. Chem.* **278**, 2396–2402
26. Hershko, A., and Ciechanover, A. (1998) *Annu. Rev. Biochem.* **67**, 425–479
27. Chan, K., Lu, R., Chang, J. C., and Kan, Y. W. (1996) *Proc. Natl. Acad. Sci. U. S. A.* **93**, 13943–13948
28. Salghetti, S. E., Muratani, M., Wijnen, H., Futcher, B., and Tansey, W. P. (2000) *Proc. Natl. Acad. Sci. U. S. A.* **97**, 3118–3123
29. Favreau, L. V., and Pickett, C. B. (1991) *J. Biol. Chem.* **266**, 4556–4561
30. Treier, M., Staszewski, L., and Bohmann, D. (1994) *Cell* **78**, 787–796
31. Moramitsu, Y., Nakagawa, Y., Hayashi, K., Fujii, H., Kumagai, T., Nakamura, Y., Osawa, T., Horio, F., Itoh, K., Iida, K., Yamamoto, M., and Uchida, K. (2002) *J. Biol. Chem.* **277**, 3456–3463
32. Bonneson, C., Eggleston, I. M., and Hayes, J. D. (2001) *Cancer Res.* **61**, 6120–6130
33. Prestera, T., Holtzclaw, W. D., Zhang, Y., and Talalay, P. (1993) *Proc. Natl. Acad. Sci. U. S. A.* **90**, 2965–2969
34. Nguyen, T., Huang, H. C., and Pickett, C. B. (2000) *J. Biol. Chem.* **275**, 15466–15473
35. Kirlin, W. G., Cai, J., Thompson, S. A., Diaz, D., Kavanagh, T. J., and Jones, D. P. (1999) *Free Radic. Biol. Med.* **27**, 1208–1218
36. Ciechanover, A. (1998) *EMBO J.* **17**, 7151–7160
37. Baumeister, W., Walz, J., Züll, F., and Seemüller, E. (1998) *Cell* **92**, 367–380
38. Glickman, M. H., and Ciechanover, A. (2001) *Physiol. Rev.* **82**, 373–428
39. Sekhar, K. R., Soltaninassab, S. R., Borrelli, M. J., Xu, Z-Q., Meredith, M. J., Domann, F. E., and Freeman, M. L. (2000) *Biochem. Biophys. Res. Commun.* **270**, 311–317
40. Pickart, C. M. (2000) *Trends Biochem. Sci.* **25**, 544–548
41. Varshavsky, A. (1996) *Proc. Natl. Acad. Sci. U. S. A.* **93**, 12142–12149
42. Lenk, U., and Sommer, T. (2000) *J. Biol. Chem.* **275**, 39403–39410
43. Blondel, M., Galan, J-M., Chi, Y., Lafourcade, C., Longaretti, C., Deshaies, R. J., and Peter, M. (2000) *EMBO J.* **19**, 6085–6097
44. Brooks, P., Fuertes, G., Murray, R. Z., Bose, S., Knecht, E., Rechsteiner, M. C., Hendil, K. B., Tanaka, K., Dyson, J., and Rivett, A. J. (2000) *Biochem. J.* **346**, 155–161
45. De Conto, F., Pilotti, E., Razin, S. V., Ferraglia, F., Géraud, G., Arcangeletti, C., and Scherrer, K. (2000) *J. Cell Sci.* **113**, 2399–2407
46. Lafarga, M., Berciano, M. T., Pena, E., Mayo, I., Castaño, J. G., Bohmann, D., Rodrigues, J. P., Tavanez, J. P., and Carmo-Fonseca, M. (2002) *Mol. Biol. Cell* **13**, 2771–2782
47. Adams, J. Kelso, R., and Cooley, L. (2000) *Trends Cell Biol.* **10**, 17–24
48. Dhakshinamoorthy, S., and Jaiswal, A. (2001) *Oncogene* **20**, 3906–3917
49. Zipper, L. M., and Mulcahy, R. T. (2002) *J. Biol. Chem.* **277**, 36544–36552
50. Jäger, S., Strayle, J., Heinemeyer, W., and Wolf, D. H. (2001) *EMBO J.* **20**, 4423–4431
51. Farber, E. (1984) *Can. J. Biochem. Cell Biol.* **62**, 486–494
52. Hayes, J. D., and McLellan, L. I. (1999) *Free Radic. Res.* **31**, 273–300
53. Sekhar, K. R., Yan, X. X., and Freeman, M. L. (2002) *Oncogene* **21**, 6829–6834

Available online at www.sciencedirect.com
SCIENCE DIRECT®
Biochemical and Biophysical Research Communications 305 (2003) 271–277
BBRC
www.elsevier.com/locate/ybbrc

Activation of Nrf2 and accumulation of ubiquitinated A170 by arsenic in osteoblasts

Junko Aono,[a] Toru Yanagawa,[a] Ken Itoh,[b] Baojie Li,[c] Hiroshi Yoshida,[a] Yoshito Kumagai,[d] Masayuki Yamamoto,[b] and Tetsuro Ishii[d,*]

[a] *Institute of Clinical Medicine, University of Tsukuba, Tsukuba, Ibaraki 305-8575, Japan*
[b] *Institute of Basic Medical Sciences, University of Tsukuba, Tsukuba, Ibaraki 305-8575, Japan*
[c] *Institute of Molecular and Cell Biology, 30 Medical Drive, Singapore, Singapore*
[d] *Institute of Community Medicine, University of Tsukuba, Tennoudai 1-1-1, Tsukuba, Ibaraki 305-8575, Japan*

Received 8 April 2003

Abstract

Sub-lethal levels of arsenic induce upregulation of stress proteins. We here report for the first time that inorganic arsenic activates the transcription factor Nrf2, which controls the expression of oxidative stress-induced proteins. Treatment of cultured MC3T3-E1 osteoblasts with arsenite or arsenate induced increase of Nrf2, followed by transcriptional activation of target genes encoding HO-1, Prx I, and A170. We found that arsenate (200–800 μM) only slightly increased the normal 60 kDa A170 protein but markedly increased higher molecular mass forms of A170 (HMM-A170) that appeared as smeared bands. Arsenate also markedly increased ubiquitin-conjugated cellular proteins, suggesting that HMM-A170 was one of the poly-ubiquitinated proteins. Arsenite (50–100 μM) also induced accumulation of HMM-A170 and ubiquitin-conjugated proteins. These results provide the first direct evidence that toxic arsenics impair the normal function of A170. Our findings provide a potential diagnostic tool for monitoring biotoxicity in cells and tissues in response to arsenic compounds.

Keywords: Nrf2; Arsenic; Osteoblast; A170; Stress protein; Ubiquitin; Heme oxygenase-1; Peroxiredoxin I

Among the chemical species of arsenic present in the environment, inorganic arsenic is generally considered the most hazardous. In general, arsenite [As(III)] is more acutely toxic than arsenate [As(V)]. As(III) is considered to react with vicinal sulfhydryl sites in proteins. As(III) modulates the cellular glutathione redox system and results in impaired removal of hydrogen peroxide and cell death [1]. Cells undergo adaptive responses to counteract these toxic effects by increasing the expression of stress proteins. Increases in the levels of heat shock proteins [2,3] and heme oxygenase-1 (HO-1) [4,5] are well-known cellular stress responses induced by arsenic and other stress agents. Increased expression of metallothionein [6] and ubiquitin [7] in tissues or cultured cells was observed following treatment with arsenic compounds. We showed previously that As(III) activated expression of a 23 kDa stress protein termed MSP23 in murine peritoneal macrophages [8]. MSP23 is now known as murine peroxiredoxin I (Prx I), an antioxidant protein with thioredoxin peroxidase activity. Transcriptional activation of the *prx I* gene is also induced by As(V) in murine osteoblasts [9]. We have previously shown that enhanced expression of HO-1 in murine peritoneal macrophages by As(III) depends largely on the transcription factor Nrf2 [10]. Nrf2 plays an integral role in the induction of genes encoding HO-1, Prx I, and A170 in macrophages. Thus, upregulation of antioxidant stress proteins may prove to be a useful tool to monitor sub-lethal toxicity of arsenics [11,12].

Ubiquitin is used as a covalent signal for selective proteolysis by 26S proteasome and for other stress responses [13]. Ligation of multiple ubiquitins to a substrate protein confers substrate recognition by an ATP-dependent protease, and ubiquitin is regenerated during degradation by one or more specific isopeptidases. It has

* Corresponding author. Fax: +81-29-853-3061.
E-mail address: teishii@md.tsukuba.ac.jp (T. Ishii).

0006-291X/03/$ - see front matter © 2003 Elsevier Science (USA). All rights reserved.
doi:10.1016/S0006-291X(03)00728-9

been reported that As(III) has a dual effect on the ubiquitin-dependent proteolytic pathway. As(III), at low concentrations (0.5–10 μM), induces accumulation of ubiquitin-conjugated proteins in tissue slices and cultured cells due to the inhibition of proteasome activity [14]. In contrast, higher concentrations (100 μM) of As(III) inhibit ubiquitination [15] by reducing the activities of ubiquitin carrier protein and aminoacyl-tRNA protein transferase [16].

In this study, we examined the effects of As(V) and As(III) on the activation of Nrf2 and expression of the stress protein A170 [17] in murine calvarial-derived osteoblast-like MC-3T3E1 cells. Expression of A170 in this cell strain was shown previously [18] and was observed to increase during differentiation of the cells to osteoblasts [19], suggesting an important role of A170 in osteogenesis. A170 belongs to a new class of ubiquitin-binding proteins with an ubiquitin interacting domain near the C-terminal. The C-terminal 100 amino acid residues of murine A170 [17] are completely conserved among other members, e.g., human p62 [20] and rat ZIP [21], suggesting that the non-covalent interaction of these proteins with ubiquitin is important for function. Notably, recent reports indicate that mutations in the ubiquitin interacting domain of the p62 gene are linked with human Paget disease [22,23].

We found that As(V) induced nuclear accumulation of Nrf2, resulting in the transcriptional activation of the target gene *A170*. Although we could not detect significant increases in normal 60 kDa A170 protein levels, we here report the first evidence for arsenic-induced formation of novel higher molecular mass forms of A170 (HMM-A170 > 65 kDa). Under experimental conditions, we found a marked accumulation of ubiquitin-conjugated cellular proteins, suggesting that HMM-A170 is one of these. Protein expression of both HMM-A170 and ubiquitin-conjugated proteins was co-induced by toxic arsenics, providing a potential diagnostic tool to monitor biotoxicity in cells and tissues in response to arsenic compounds.

Materials and methods

Chemicals. Sodium arsenate, sodium arsenite, cadmium chloride, diethylmaleate, and paraquat were purchased from Wako Pharmaceutical (Tokyo). An anti-actin rabbit antiserum (A2066) and culture media were from Sigma (Tokyo). An anti-ubiquitin rabbit antiserum (Z0458) was from Dako (Tokyo). MG132 was from Protein Institute (Osaka). Fetal bovine serum was from Hyclone (Logan).

Cell culture and immunostaining. MC3T3-E1 cells were cultured in αMEM containing 10% (v/v) fetal bovine serum, 50 U/ml penicillin, and 50 μg/ml streptomycin. Cell viability was measured by the MTT assay [24]. To isolate nuclear extracts, cells were scraped off and collected by centrifugation in PBS. The nuclear pellets were prepared after the cell lysis in 0.5% Nonidet P-40 containing buffer [25]. For the detection of intracellular localization of the proteins, the cells were fixed with 4% paraformaldehyde, stained either with anti-ubiquitin or anti-A170, and reacted with a FITC-conjugated secondary antibody. The immunofluorescence was observed using a microscope (Leica DM IRE2).

Immunoblotting. Cultured cells were solubilized with SDS-sample buffer (50 mM Tris–HCl, pH 6.8, 2% SDS, and 10% glycerol), and protein concentrations were estimated by BCA protein assay (Pierce). The proteins were separated by SDS–polyacrylamide gel electrophoresis in the presence of 2-mercaptoethanol and electrotransferred onto Immobilon-P membrane (Millipore). To detect immunoreactive proteins, we used horseradish peroxidase-conjugated anti-rabbit IgG and ECL blotting reagents (Amersham Pharmacia Biotech). Polyclonal rabbit antisera raised against recombinant murine A170 and rat HO-1 were used.

Northern blotting. Total cellular RNA was extracted from cells by RNeasy (Bio-Rad). The RNA samples (10 μg) were electrophoresed and transferred to Zeta-Probe GT membranes (Bio-Rad). Membranes were probed with ^{32}P-labeled cDNA probes as indicated in the figure legends.

Percoll density gradient fractionation. We used the procedure described by Carlsson and Fukuda [26]. All procedures were performed at 0–4 °C. Cells treated with 800 μM As(V) for 16 h were washed three times in PBS and scraped off from culture dishes, collected by centrifugation at 500*g* for 10 min. The cells were washed once in homogenization medium (0.25 M sucrose, 1 mM Na_2EDTA, and 20 mM Hepes, pH 7.0), suspended in the medium containing 1% (v/v) protease inhibitor cocktail (Sigma), and homogenized using Potter type homogenizer [26]. Homogenates were centrifuged at 800*g* for 10 min. The supernatant was mixed with Percoll stock solution to make 20% (v/v) Percoll containing homogenization medium. The solution was centrifuged in a swing rotor (Beckman SW40) at 16,000 rpm for 30 min and fractionated from the bottom of the tube every 0.5 ml. To collect and analyze the proteins in each fraction, 0.1 ml portions were taken into tubes, mixed with 0.1 ml ovalbumin (2 mg/ml) to which was added 0.2 ml of 10% TCA, and kept on ice for 10 min to precipitate proteins. Acid precipitates were collected by centrifugation and neutralized with bicarbonate before analysis with SDS–PAGE.

Results

Activation of Nrf2 by As(V) and As(III)

We examined the effects of As(V) and As(III) on Nrf2 activation in MC-3T3E1 cells. Nrf2 protein levels were monitored in both total cell protein lysates and nuclear fractions (Figs. 1A and B). Treatment of cells with 800 μM As(V) induced a marked increase in Nrf2 levels in total cell lysates within 4 h, peaking at 16 h and remaining elevated up to 24 h. Nuclear Nrf2 levels were also increased several fold after 5 h treatment with either 200 or 400 μM As(V) (Fig. 1B). These results indicate that As(V) causes a rapid and long lasting increase in Nrf2 levels. In contrast to As(V), the effects of 100 μM As(III) caused a delayed increase in Nrf2 levels, reaching a maximum at 12 h and subsequently decreasing to control levels after 24 h (Fig. 1A).

Since the activation of the transcription enhancer Nrf2 upregulated expression of genes encoding HO-1, Prx I, and A170 in murine macrophages [10], we conducted Northern blot analyses using total RNA from the cells treated for 5 h in the absence or presence of 200 μM As(V). As expected from previous studies, As(V) treatment markedly increased mRNA levels of HO-1 and Prx I

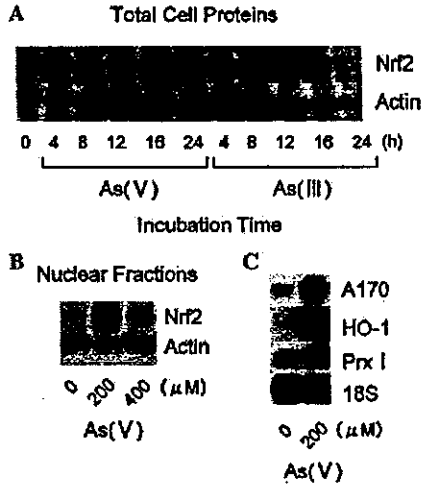

Fig. 1. Arsenic-induced accumulation of Nrf2 in the osteoblasts and transcriptional activation of the target stress genes. (A) Immunoblot analysis to detect increase of Nrf2 protein levels in total cell proteins prepared after the treatment of cells either with 800 μM As(V) or 100 μM As(III) for 0, 4, 8, 12, 16, and 24 h, respectively. Actin was used as an internal control. (B) Immunoblot analysis to detect accumulation of Nrf2 in nuclear fractions after the treatment of the cells with 200 and 400 μM As(V) for 5 h. (C) Northern blot analysis to detect activation of genes encoding A170, HO-1, and Prx I. 18S ribosome was used as an internal control.

(Fig. 1C). To our knowledge, our results provide the first evidence that As(V) also upregulates A170 mRNA levels 2.9 ± 0.3 fold (mean ± SEM, $n = 3$ different cell cultures).

Formation of high molecular mass forms of A170 in cells treated with As(V)

We next examined the effects of As(V) on A170 and HO-1 expression in MC3T3-E1 cells by immunoblotting. We observed that As(V) increased HO-1 levels in a dose-dependent manner (Fig. 2A), which served as a positive control of the cellular stress response induced by As(V). In contrast to the marked increase of HO-1 expression, A170 protein levels (normal 60 kDa and smaller related 53 kDa protein) were only marginally increased after exposure of cells to As(V) (50–400 μM) for 16 h (Fig. 2A). However, the antibody also cross-reacted with molecular mass forms >65 kDa that appeared as smeared bands, which we here term HMM-A170 (high molecular mass forms of A170 >65 kDa). Since the smeared banding pattern resembled those for ubiquitin-modified proteins, we blotted the same lysates with an anti-ubiquitin antibody and found a marked accumulation of ubiquitin-conjugated proteins from cells treated with 300–400 μM As(V) (Fig. 2A, right-hand panel). The banding patterns in membranes stained with anti-ubiquitin were quite similar to those for HMM-A170. This result indicates for the first time that the treatment of MC3T3-E1 with As(V) induces accumulation of ubiquitinated proteins.

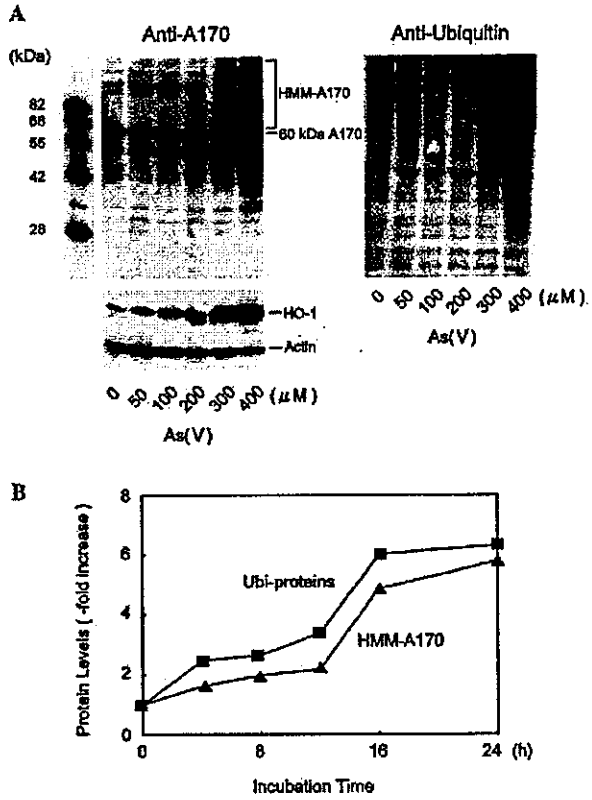

Fig. 2. As(V) accumulates high molecular mass forms of A170 in the cells. (A) Immunoblot analysis to detect accumulation of high molecular mass forms of A170 (HMM-A170) and ubiquitin-conjugated cellular proteins after the treatment of cells for 16 h with 0, 50, 100, 200, 300, and 400 μM As(V). The whole cell proteins were separated with SDS–PAGE and immunoblotted either with the A170-specific, HO-1-specific or actin-specific antibodies (left panel) or ubiquitin-specific antibody (right panel). (B) Time-dependent formation of both HMM-A170 and ubiquitin-conjugated cell proteins during treatment of the cells with 400 μM As(V). The immunostained protein bands (>65 kDa) were, respectively, integrated using the NIH image software. Values represent relative amounts of the immunoblotted proteins.

We then examined the time-dependent formation of both HMM-A170 and ubiquitinated proteins during the treatment of the cells with As(V) for up to 24 h (Fig. 2B). Protein bands above 65 kDa were quantitated by densitometry using NIH image software. The formation of both high molecular forms was slow in onset over the first 12 h, increased markedly between 12 and 16 h, reaching maximal levels between 16 and 24 h (Fig. 2B). In another subset of experiments we established that the critical concentration of As(V) required to induce formation of HMM-A170 ranged between 200 and 400 μM depending on culture conditions. Under our culture conditions, cell viability decreased by 30–50% (measured by MTT assay) after the treatment of cells with As(V) for 24 h. The loss of cell viability coincided with the formation of HMM-A170 and ubiquitin-conjugated proteins. It is worth noting that the formation of these

high molecular mass proteins always occurred in parallel, irrespective of the cell culture conditions or stimuli tested. It seems reasonable to conclude from these results that HMM-A170 is one of the ubiquitin-conjugated proteins induced in MC3T3-E1 cells by As(V).

Intracellular localization of HMM-A170 and ubiquitin-conjugated proteins

We next monitored their intracellular distributions by immunostaining As(V)-treated cells with A170- and ubiquitin-specific antibodies. In the absence of As(V), both anti-A170 and anti-ubiquitin antibodies faintly stained the cytoplasm with small spots. However, after the treatment with As(V), the cytoplasm was heavily stained, but unevenly, with anti-A170 (Fig. 3), suggesting that HMM-A170 is associated with intracellular organelles within the cytoplasm. To characterize the HMM-A170 associated cytoplasmic structures, we separated cell homogenates by Percoll density gradient centrifugation. The fractions were collected from bottom of the tube and analyzed by immunoblotting as described in Materials and methods. This Percoll gradient system separates dense lysosomes (near bottom) from lighter particles such as ER, plasma membrane, and Golgi (near top). We found that 60 kDa A170 was distributed among all fractions, suggesting that it does not physically associate with HMM-A170. In contrast, HMM-A170 was mainly recovered in the top fraction (Fraction No. 19, see Fig. 4), suggesting that HMM-A170 associates with particular structures having a low

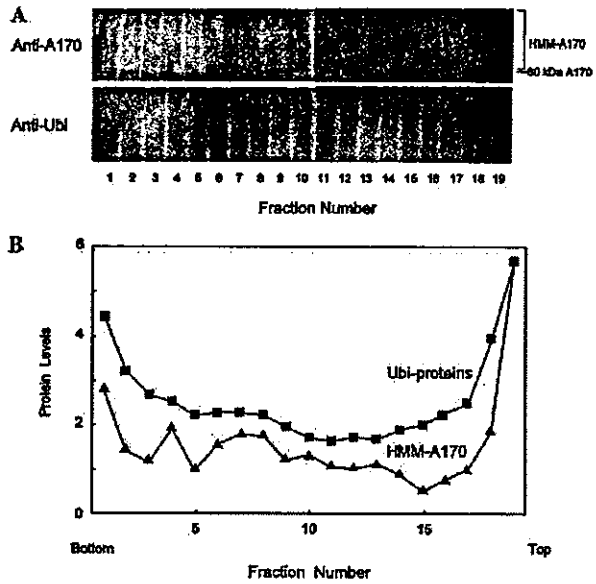

Fig. 4. Fractionation of A170 and ubiquitinated proteins in cell homogenates by a Percoll density gradient. The cells treated with 800 μM As(V) for 16 h were collected, homogenized, and centrifuged in 20% (v/v) Percoll containing medium to fractionate sub-cellular organelles [26]. Fractions (each 0.5 ml) were collected from the bottom of the tubes. The proteins in the fractions were, respectively, collected by precipitation with TCA using ovalbumin as a carrier as described in Materials and methods. Upper panels: immunoblot analysis of proteins in the fractions after SDS–PAGE with anti-A170 (upper) and anti-ubiquitin. Lower panel: quantitation of relative amounts of HMM-A170 (filled triangle) and ubiquitin-conjugated proteins (filled square). This Percoll gradient system separates dense lysosome (near bottom) from ER, plasma membrane, and Golgi (near top).

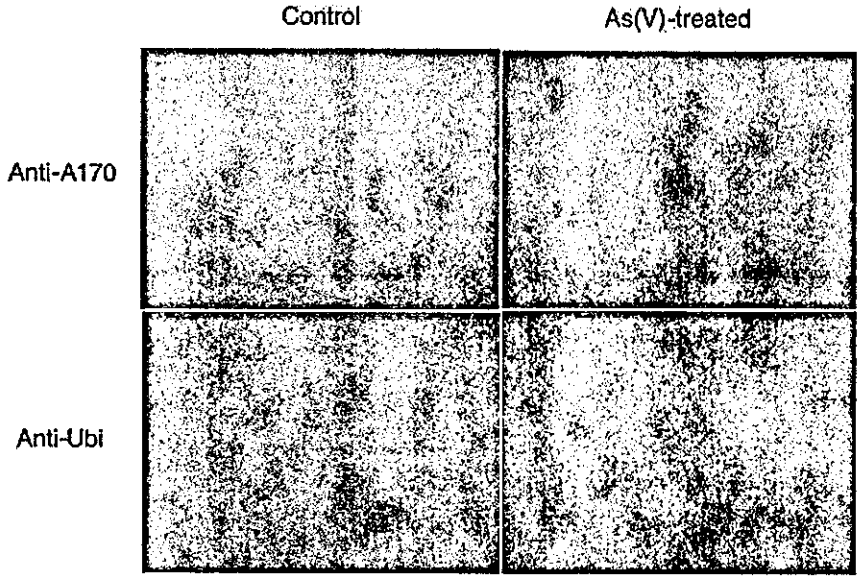

Fig. 3. Localization of A170, HMM-A170, and ubiquitin in the cells before and after the treatment with As(V). The cells were treated with 800 μM As(V) for 16 h and fixed and stained with each specific antibody as described in Materials and methods. FITC-labeled secondary antibody showed accumulation of both proteins in cytoplasm.

density. The ubiquitin-conjugated proteins were distributed in all fractions but the contents were especially high in both top and bottom fractions. These results indicate that the major fractions of HMM-A170 and ubiquitin-conjugated cellular proteins co-localize in low density sub-cellular particulate structures distinct from dense lysosomes.

Effects of other stress agents and proteasome inhibitor MG132 on HMM-A170 formation

We next examined the effects of As(III) and other stress agents on the formation of HMM-A170 and ubiquitin-conjugated proteins. We found that As(III) (50–100 μM) also induced formation of both types of proteins (Fig. 5A). Notably treatment of cells with 200 μM As(III) showed smaller effects. We could not detect formation of HMM-A170 in the cells treated with 400–1000 μM dimethylarsinic acid or methylarsonic acid (data not shown). These methylated arsenic compounds were not toxic to cells as judged by the MTT assay after incubation for 24 h (data not shown). These results suggest that formation of HMM-A170 and ubiquitin-conjugated proteins is associated with the cytotoxicity of arsenic.

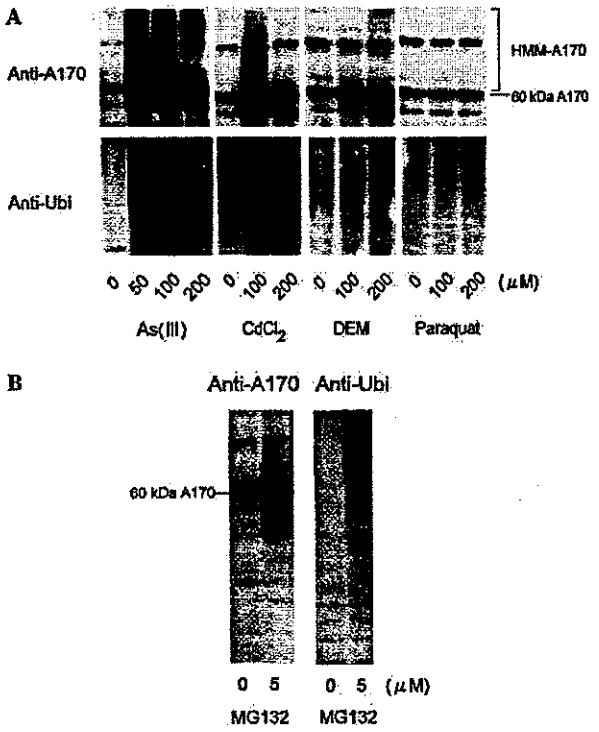

Fig. 5. Immunoblot analysis to examine the effects of As(III) and other chemical agents on the formation of HMM-A170 and ubiquitin-conjugated cellular proteins. (A) The cells were treated either with As(III) (50, 100, and 200 μM), cadmium chloride (100 and 200 μM), diethylmaleate (DEM; 100 and 200 μM), and paraquat (100 and 200 μM) for 16 h. (B) The cells were treated with MG132 (5 μM) for 16 h.

When we examined the effects of other stress agents in MC3T3-E1 cells, we found that $CdCl_2$ showed similar dose-dependent effects to As(III) on the formation of HMM-A170 and ubiquitin-conjugated proteins. $CdCl_2$ was only effective at increasing formation of HMM-A170 at 100 μM and less effective at 200 μM. A typical Nrf2 activating electrophilic agent, diethylmaleate, enhanced expression of 60 kDa A170 at 100 and 200 μM and hardly enhanced formation of HMM-A170 and ubiquitin-conjugated proteins (Fig. 5A). The superoxide generating agent paraquat (100 and 200 μM) did not induce formation of either 60 kDa A170 or HMM-A170 (Fig. 5A). The proteasome inhibitor MG132 increased formation of ubiquitin-conjugated proteins and 60 kDa A170 but hardly increased HMM-A170 (Fig. 5B). These results suggest that only arsenic and Cd cause marked formation of both HMM-A170 and ubiquitin-conjugated proteins.

Discussion

Accumulation of HMM-A170 and/or ubiquitin-conjugated cellular proteins in cells exposed to arsenic may serve as a novel bio-marker of environmental metal poisoning. Contamination of non-organic arsenic compounds in drinking water causes serious health problems in Asian countries such as Bangladesh and China [27,28]. Long-term exposure to ingested arsenic induces skin cancers, peripheral vascular disease, ischemic heart disease, and cerebral infarction [29], yet the molecular mechanism(s) underlying the toxic effects of arsenics remain to be elucidated.

We have studied the effects of arsenic compounds on activation of the transcription factor Nrf2 and expression of stress proteins A170 and ubiquitin in murine MC3T3-E1 cells and obtained the following novel results: (i) As(V) and As(III) upregulate Nrf2 levels in nuclear and whole cell fractions, leading to the activation of target stress genes (Fig. 1), (ii) As(V) induces a dose- and time-dependent accumulation of both ubiquitin-conjugated cellular proteins and high molecular mass forms of A170 termed HMM-A170 (Fig. 2), (iii) most of HMM-A170 and a fraction of ubiquitin-conjugated cellular proteins are co-localized in sub-cellularly distinct from dense lysosomes (Figs. 3 and 4), and (iv) low concentrations of As(III) and $CdCl_2$ induce accumulation of both proteins (Fig. 5A).

We have shown for the first time that both As(V) and As(III) activate Nrf2 in cultured MC3T3-E1 osteoblasts. These results are consistent with our previous report that As(III) increases the expression of HO-1 by an Nrf2-dependent manner in murine peritoneal macrophages [10]. Nrf2 has a short half-life due to proteasome-mediated degradation, however, stress agents interact with the Nrf2–Keap1 sensor system to release Nrf2 from Keap1, thereby stabilizing Nrf2 [30].

Notably, treatment of cultured cells with a proteasome-specific inhibitor MG132 induces accumulation of Nrf2 and mimics the effects of other stress agents [30]. Since low levels As(III) inhibit the activity of 20S proteasome resulting in the accumulation of ubiquitin-conjugated proteins [14], our results suggest that As(V), over a wide range of concentrations (200–800 μM), also inhibits proteasome activity in a manner similar to As(III), resulting in accumulation of Nrf2. Although As(V), similar to MG132, causes accumulation of ubiquitin-conjugated proteins, the formation of HMM-A170 by the As(V) was not simply due to the inhibition of proteasome activity because treatment with MG132 has no effect on HMM-A170 accumulation in the cells (Fig. 5B). These results suggest that As(V) may also inhibit de-ubiquitination and thereby enhance accumulation of ubiquitin-conjugated proteins.

We have detected for the first time the high molecular mass form of A170, which appeared to be one of the ubiquitin-conjugated cellular proteins induced in response to arsenic treatment. This hypothesis is based on the following observations that the banding pattern and sub-cellular localization of HMM-A170 are quite similar to those of ubiquitin-conjugated proteins. Moreover, A170 belongs to a new class of ubiquitin-binding proteins having a high affinity for ubiquitin [20]. The formation of HMM-A170 and ubiquitin-conjugated proteins depends on the toxicity of arsenic compounds. Limited formation of HMM-A170 was seen on exposure to 400–1000 μM monomethylarsonic acid or dimethylarsinic acid (data not shown). Since methylated arsenates are known to be detoxification products of inorganic arsenicals [31], they thus may not induce ubiquitination of proteins.

Our findings have identified an important role for Nrf2 in arsenic-induced upregulation of the stress proteins in osteoblasts. Notably, a recent report shows that Nrf2 plays a key role in the expression of ubiquitin [32]. We have shown that environmental metal pollutants such as arsenics and Cd cause a marked ubiquitination of A170 and other proteins, leading to the inactivation of A170 and ubiquitin. As A170/p62 is expected to play roles in defense against stress-induced misfolded proteins [33] and in PKC-ζ-mediated signaling pathways [34], this could limit the cellular antioxidant defenses of cells against metal poisoning. Our findings also offer the potential for developing a sensitive and specific detection system to monitor the formation of ubiquitin-conjugated proteins as an assay for metal toxicity in plasma and blood cells from patients.

Acknowledgments

The authors thank Dr. Y. Amagai and Dr. S. Taketani for providing MC3T3-E1 cells and anti-HO-1 antibody, respectively. We thank Prof. G.E. Mann and Prof. N. Simojo for their helpful discussions during our study. We thank Ms. Y. Yamagishi for her able technical assistance. This study was supported in part by Grants-in-aid from the Ministry of Education, Science, Sports and Culture in Japan, University of Tsukuba Research Projects, and the COE program in year 2001.

References

[1] Y. Jing, J. Dai, R.M.E. Chalmers-Redman, W.G. Tatton, S. Waxman, Arsenic trioxide selectively induces acute promyelocytic leukemia cell apoptosis via a hydrogen peroxide-dependent pathway, Blood 94 (1999) 2102–2111.

[2] C. Wang, R.H. Gomer, E. Lazarides, Heat shock proteins are methylated in avian and mammalian cells, Proc. Natl. Acad. Sci. USA 78 (1981) 3531–3535.

[3] M.E. Mirault, R. Southgate, E. Delwart, Regulation of heat-shock genes: a DNA sequence upstream of *Drosophila* hsp70 genes is essential for their induction in monkey cells, EMBO J. 1 (1982) 1279–1285.

[4] M.K. Sardana, G.S. Drummond, S. Sassa, A. Kappas, The potent heme oxygenase inducing action of arsenic and parasiticidal arsenicals, Pharmacology 23 (1981) 247–253.

[5] M.E. Cebrian, A. Albores, J.C. Connelly, J.W. Bridges, Assessment of arsenic effects on cytosolic heme status using tryptophan pyrrolase as an index, J. Biochem. Toxicol. 3 (1988) 77–86.

[6] T. Maitani, N. Saito, M. Abe, S. Uchiyama, Y. Saito, Chemical form-dependent induction of hepatic zinc-thionein by arsenic administration and effect of co-administered selenium in mice, Toxicol. Lett. 39 (1987) 63–70.

[7] U. Bond, N. Ageli, A.L. Haas, K. Redman, M.J. Schlesinger, Ubiquitin in stressed chicken embryo fibroblasts, J. Biol. Chem. 263 (1988) 2384–2388.

[8] T. Ishii, M. Yamada, H. Sato, M. Matsue, S. Taketani, K. Nakayama, Y. Sugita, S. Bannai, Cloning and characterization of a 23-kDa stress-induced mouse peritoneal macrophage protein, J. Biol. Chem. 268 (1993) 18633–18636.

[9] L. Baojie, T. Ishii, C.P. Tan, J.-W. Soh, S.P. Goff, Pathways of induction of peroxiredoxin I expression in osteoblasts: role of p38 mitogen-activated protein kinase and protein kinase C, J. Biol. Chem. 277 (2002) 12418–12422.

[10] T. Ishii, K. Itoh, S. Takahashi, H. Sato, T. Yanagawa, Y. Katoh, S. Bannai, M. Yamamoto, Transcription factor Nrf2 coordinately regulates a group of oxidative stress-inducible genes in macrophages, J. Biol. Chem. 275 (2000) 16023–16029.

[11] L.M. Del-Razo, B. Quintanilla-Vega, E. Brambila-Colombres, E.S. Calderon-Aranda, M. Manno, A. Albores, Stress proteins induced by arsenic, Toxicol. Appl. Pharmacol. 177 (2001) 132–148.

[12] J. Liu, M.B. Kadiiska, Y. Liu, T. Lu, W. Qu, M.P. Waalkes, Stress-related gene expression in mice treated with inorganic arsenicals, Toxicol. Sci. 61 (2001) 314–320.

[13] A. Hershko, A. Ciechanover, The ubiquitin system, Annu. Rev. Biochem. 67 (1998) 425–479.

[14] D.S. Kirkpatrick, K.V. Dale, J.M. Catania, A.J. Gandolfi, Low-level arsenite causes accumulation of ubiquitinated proteins in rabbit renal cortical slices and HEK293 cells, Toxicol. Appl. Pharmacol. 186 (2003) 101–109.

[15] N.S. Klemperer, C.M. Pickart, Arsenite inhibits two steps in the ubiquitin-dependent proteolytic pathway, J. Biol. Chem. 264 (1989) 19245–19252.

[16] N.S. Klemperer, E.S. Berleth, C.M. Pickart, A novel arsenite-sensitive E2 of the ubiquitin pathways: purification and properties, Biochemistry 28 (1989) 6035–6041.